




## Exosome-loaded tannic acid–thioctic acid hydrogel enhances wound healing in coagulation disorders

Yuesheng Tu<sup>a,1</sup>, Weixin Zheng<sup>a,1</sup>, Zichu Ding<sup>a,1</sup>, Jie Xiang<sup>d</sup>, Qinfeng Yang<sup>b</sup>, Yuchen Liu<sup>a</sup>, Jue Cao<sup>a</sup>, Yuling Shen<sup>a</sup>, Zinan Tang<sup>a</sup>, Shen Lin<sup>a</sup>, Lei Fan<sup>b,\*\*\*</sup>, Yaowen Xu<sup>c,\*\*</sup>, Bin Chen<sup>a,\*</sup> 

<sup>a</sup> Division of Orthopaedics and Traumatology, Department of Orthopaedics, Nanfang Hospital, Southern Medical University, Guangzhou, Guangdong, 510515, China

<sup>b</sup> Division of Orthopaedic Surgery, Department of Orthopaedics, Nanfang Hospital, Southern Medical University, Guangzhou, Guangdong, China

<sup>c</sup> Department of Health Management, Nanfang Hospital, Southern Medical University, Guangzhou, Guangdong, 510515, China

<sup>d</sup> Department of Orthopaedics and Traumatology, The First Affiliated Hospital, Hengyang Medical School, University of South China, China

### ARTICLE INFO

#### Keywords:

Hydrogel  
Exosome  
Wound healing  
Delivery  
Inflammation

### ABSTRACT

Hemophilia poses distinct challenges to wound healing, primarily due to uncontrolled bleeding and delayed tissue repair. This study explored a novel tannic acid-thioctic acid (TATA) hydrogel, enriched with exosomes derived from bone marrow mesenchymal stem cells, as a therapeutic strategy for enhancing skin wound healing in a hemophilia model. The hydrogel exhibited robust hemostatic efficacy, potent antioxidant activity, and the capacity to modulate the inflammatory microenvironment. Both *in vitro* and *in vivo* assessments demonstrated significantly accelerated wound closure, increased collagen deposition, and pronounced angiogenesis in the TATA Hydrogel-Exosome (TATA Hydrogel-Exos) treatment group relative to controls. Rheological evaluations confirmed the self-healing properties and mechanical durability, of the hydrogel, underscoring its potential for sustained therapeutic application. Importantly, no significant systemic toxicity was observed, indicating favorable biocompatibility. These multifunctional TATA Hydrogel-Exos present a promising therapeutic avenue for hemophilia-related wounds by integrating hemostasis, inflammation regulation, and tissue regeneration.

### 1. Introduction

Hemophilia encompasses a spectrum of inherited genetic disorders that impair the body's ability to form blood clots, resulting in prolonged bleeding episodes [1,2]. Although hemophilia is predominantly associated with internal bleeding and deep muscle hemorrhages, it also poses notable challenges to cutaneous wound healing [3–7]. Conventional treatments primarily focus on replenishing deficient clotting factors, however, they fail to address the intricate biological processes critical for effective tissue repair [4,5,8–10]. Thus, innovative therapeutic strategies are urgently needed that not only correct the underlying coagulation deficiencies but also actively promote wound healing mechanisms.

In recent years, hydrogels have emerged as promising materials in wound healing due to their biocompatibility, tunable mechanical properties, and capacity for controlled drug delivery [11,12].

Traditional hemostatic methods, such as gauze compression, hemostatic powders, and gelatin sponges, while widely used for their accessibility and simplicity, often face limitations, including insufficient adhesion to irregular wound surfaces, lack of bioactive functionality, and risks of secondary injury during removal [13,14]. For instance, gauze compression relies on external pressure, which may be ineffective in controlling severe bleeding or addressing wounds with complex geometries [14]. In contrast, multifunctional hydrogels, such as the hydrogel in our study, not only offer robust hemostatic properties through mechanical adhesion and biochemical pathways but also enhance wound healing by promoting angiogenesis, modulating inflammation, and delivering bioactive agents like exosomes. Exosomes, as mediators of intercellular communication, encapsulate and deliver bioactive molecules such as proteins, lipids, and nucleic acids, offering sustained therapeutic effects while improving cell activity and tissue repair. By integrating exosomes, hydrogels provide structural support and

\* Corresponding author.

\*\* Corresponding author.

\*\*\* Corresponding author.

E-mail addresses: [fanl1006@163.com](mailto:fanl1006@163.com) (L. Fan), [xuyw@smu.edu.cn](mailto:xuyw@smu.edu.cn) (Y. Xu), [chb@smu.edu.cn](mailto:chb@smu.edu.cn) (B. Chen).

<sup>1</sup> Authors contributed equally to this work.

precisely regulate the wound healing process. Furthermore, their viscoelastic properties ensure adhesion to irregular surfaces, and their controlled release of therapeutic molecules addresses both hemostasis and tissue regeneration comprehensively [11,12]. These advantages position hydrogels as a superior alternative to conventional hemostatic methods, particularly in complex clinical scenarios requiring both bleeding control and tissue repair.

Inflammation and hemostasis are fundamental aspects of the wound-healing process [15–17]. However, excessive inflammation and the accumulation of reactive oxygen species (ROS) can hinder repair, resulting in delayed healing and suboptimal outcomes [16,18]. Recent advances in biomaterials and nanotechnology have facilitated the development of innovative therapeutics that can precisely modulate these key processes [19]. Among these, hydrogels have attracted significant interest because of their biocompatibility, tunable physical properties, and capacity for therapeutic molecule delivery [20,21]. Tannic acid and thioctic acid are promising compounds for wound healing research [22–24]. Tannic acid, a polyphenol composed of five aromatic rings, each terminated by hydroxyl groups, exhibits potent antioxidant, anti-inflammatory, and hemostatic effects, making it an ideal candidate for wound treatment [25,26]. The pyrogallol moieties in tannic acid facilitate strong tissue adhesion upon oxidation, thereby enhancing its therapeutic efficacy [27,28]. Through various non-covalent interactions, tannic acid favors condensation over network formation in hydrogels and can disrupt disulfide bonds in proteins, promoting the binding of sulfur-containing molecules to phenolic structures [29,30]. Tannic acid has been combined with thioctic acid to develop a robust polymeric network, tannic acid was combined with thioctic acid [31]. Upon heating to 70 °C, thioctic acid undergoes disulfide bond cleavage within its pentacyclic ring structure, generating thioalkane radicals that initiate ring-opening polymerization [32]. This process yields a sulfur-rich linear polymer that exhibits macroscopic viscous fluid behavior [32,33]. At elevated temperatures, tannic acid and thioctic acid react to form a viscous sulfur-containing polymer, synergistically combining the advantageous properties of polyphenols and polysulfides [31].

Bone marrow mesenchymal stem cells (BMSCs) are multipotent progenitors with the capacity to differentiate into various cell types, rendering them invaluable for applications in tissue engineering and regenerative medicine [34,35]. The BMSCs contribute to tissue repair and modulate inflammation by secreting cytokines and other immunomodulatory molecules [36,37]. The immunomodulatory properties of exosomes secreted by BMSCs is a promising area of research [38,39]. Exosomes are nano-sized extracellular vesicles, typically ranging from 30 to 150 nm, that encapsulate proteins, lipids, and nucleic acids, which can influence the function of recipient cells [40–42]. These lipid-bilayer vesicles typically range from 30 to 150 nm in size [42]. These lipid-bilayered vesicles are secreted by numerous cell types and present in various bodily fluids, including blood, urine, and saliva [43]. Exosomes derived from BMSCs retain many characteristics of their parental cells, including the expression of surface markers and the ability to transport bioactive cargo such as proteins, lipids, and nucleic acids [44,45]. This cargo can be delivered to target cells by altering their physiological behavior. Studies have shown that BMSC-derived exosomes are enriched in immunoregulatory proteins and microRNAs, that can modulate immune cell activity. These exosomes play a pivotal role in inflammation regulation [46]. The immunomodulatory potential of BMSC-derived exosomes makes promising therapeutic platforms for the treatment of immune-mediated disorders and conditions that require immune modulation.

This study evaluated the efficacy of a tannic acid–thioctic acid hydrogel loaded with exosomes in promoting skin wound healing in a hemophilic model. By examining the dual impact of the hydrogel on inflammation and hemostasis, this study aimed to provide a comprehensive understanding of its therapeutic potential and lay the groundwork for its future clinical application in the treatment of hemophilia-

related wounds.

## 2. Methods

### 2.1. Cell culture

Human umbilical vein endothelial cells (HUVECs) were obtained from Procell and cultured in an endothelial cell medium (ECM) (Procell, CM-H082) supplemented with 10 % exosome-free fetal bovine serum (FBS, Gibco, USA) and 1x penicillin-streptomycin. The cells were maintained in a humidified incubator at 37 °C with 5 % CO<sub>2</sub>. NCTC clone 929 (L-929) and mouse monocytic macrophage leukemia cell line (RAW264.7), sourced from the ATCC cell bank, were cultured in high-glucose Dulbecco's modified Eagle's medium (DMEM) (Gibco, USA) under the same incubation conditions. BMSCs were isolated by flushing the bilateral femurs and tibias of two-week-old Sprague-Dawley rats with phosphate-buffered saline (PBS, Gibco, USA) under sterile conditions [47]. The BMSCs were subsequently cultured in DMEM (Gibco, USA) containing 10 % exosome-free FBS and 1x penicillin-streptomycin.

### 2.2. Characterization and validation of BMSCs and their exosome derivatives

After three passages, flow cytometry was performed to assess the surface marker expression of the isolated BMSCs using antibodies specific to CD34, CD35, CD90, and CD109 Proteintech (China) [47]. Further characterization and verification of BMSC identity was performed using Oil Red O, Alizarin Red, and Alcian Blue staining, which confirmed their differentiation potential into adipocytes, osteoblasts, and chondrocytes, respectively [47].

BMSCs were isolated and cultured in low-glucose DMEM (Gibco) supplemented with 10 % exosome-free FBS (Gibco) for 2 to 6 passages. As described in previous studies, when cell confluence reached 50%–60 %, the supernatant was collected and processed using gradient centrifugation [48]. The supernatant was sequentially centrifuged at 300 g, 3000 g, and 10,000 g for 10 min to eliminate dead cells and debris, followed by ultracentrifugation at 100,000 g for 90 min. The exosome pellet formed at the bottom of the tube was resuspended in PBS and stored at –80 °C. All centrifugation steps were performed at 4 °C. Nanoparticle tracking analysis (NTA) was used to determine the size of the exosomes and their morphology was assessed using transmission electron microscopy (TEM, JEM-1200EX, JEOL, Japan). Western blotting (WB) was used to detect exosome surface markers, including CD63, TSG101, and Alix (ProteinTech, China) [47,49,50]. The exosomes were labeled with the red fluorescent dye PKH26 (Sigma-Aldrich, USA) for further analysis.

#### 2.2.1. Exosome release *in vitro*

Exosome release was quantified using a bicinchoninic acid (BCA) assay kit (Beyotime, China) [48]. For this analysis, 100 μL of the TATA-Exos hydrogel containing 200 μg of exosomes was utilized. Three replicates of the hydrogel were incubated in PBS at 37 °C, with exosome release measured at 0, 1, 3, 5, 7, 10, and 14 d to assess the release profile. The total exosome load within the hydrogel was determined by subtracting the amount of exosomes released into PBS from the initial exosome content [48].

#### 2.2.2. Phagocytosis of exosomes

To assess whether HUVECs, RAW264.7 cells, and L929 cells could internalize the exosomes released by TATA Hydrogels, the cells were co-cultured with TATA-Exos for 24 h. Following incubation, the cells were fixed with 4 % paraformaldehyde for 30 min and subsequently treated with a solution containing 0.2 % Triton-100 × (Biofroxx, Germany) and 3 % bovine serum albumin (BSA, Biofroxx, Germany) at 37 °C for 1 h. Afterward, β-Actin Tracker Green (Beyotime, China) was applied to stain the cells for 1 h, and the nuclei were counterstained with Hoechst 33342

(Sigma, USA) for 5 min. The cellular uptake of exosomes was visualized using a laser scanning confocal microscope (ZEISS LSM 980, Germany).

### 2.3. Synthesis of TATA Hydrogel

#### 2.3.1. Preparation of poly (thioctic acid)

To prepare the poly(thioctic acid) (poly(TA)) solution, 1 g of Tris base [2-Amino-2-(hydroxymethyl)-propane-1,3-diol, Tris base, Bio-Froxx] was dissolved in four parts distilled water at 60 °C in a 100 mL beaker, using a magnetic stirrer set at a speed of 20 rpm. Subsequently, 2 g of thioctic acid [(R)-(+)- $\alpha$ -Lipoic acid, Aldrich] was added, and the mixture was heated to 70 °C while increasing the magnetic stirrer speed to 40 rpm, stirring until it reached a viscous consistency. The resulting solution was then frozen at  $-20 \pm 3$  °C for 1 h, followed by thawing at 25 °C for 1 h to yield the poly(TA) solution [31].

#### 2.3.2. Preparation of TATA hydrogel

To prepare solution A, 200–1000 mg of tannic acid and 1 g triethylamine were dissolved in 4 mL of distilled water at 60 °C in a 100 mL beaker [31]. Subsequently, 2 g of thioctic acid was added to solution A and stirred at 40 rpm using a magnetic stirrer for 30 min to obtain solution B. Solution B was then heated to 70 °C and stirred vigorously for 60 min until it became viscous. This viscous solution was transferred into a polypropylene mold or an aluminum tube and frozen at  $-20 \pm 3$  °C for 1 h. After freezing, the mixture was thawed at 25 °C for 1 h, resulting in the formation of the TATA Hydrogel [31].

#### 2.3.3. Equilibrium swelling measurement of TATA hydrogels

A 100 mg sample of the freeze-dried TATA Hydrogel was weighed and subsequently immersed in distilled water at room temperature. Once the hydrogel reached the swelling equilibrium, its surface was gently blotted with filter paper to remove excess water, and the swollen hydrogel was reweighed. The water absorption capacity was calculated using the following formula:

$$\text{Swelling}(\%) = \left( \frac{m_s - m_d}{m_d} \right) \times 100\%$$

where,  $m_d$  and  $m_s$  represent the initial dry weights of the hydrogel before and after swelling, respectively [51].

#### 2.3.4. Rheological and material characterization of the hydrogels

A rheometer (HAAKE MARS 40, Thermo Scientific) equipped with a 40 mm cone plate and a 1° cone angle was used to gradually increase the strain from 0.1 % to 1000 %, while monitoring strain rupture across a range of temperatures (25, 37, 50, 75, and 90 °C) to encompass a broad thermal spectrum. The angular frequency was maintained at 10 rad/s. Frequency sweep tests were conducted to assess the hydrogel's response across different frequencies. At the specified temperatures, the frequency was incrementally increased from 0.1 to 100 Hz, with strain fixed at 1 %, to monitor strain rupture. Step-cycle tests were performed at a constant temperature of 37 °C and 10 rad/s to further investigate the rheological characteristics of the hydrogel.

The UV–visible spectra of the hydrogel and its oxidation products were recorded using a UV–Vis spectrophotometer (Thermo Scientific). To prepare the samples, the hydrogel was dissolved in distilled water at a concentration of 1 mg/mL. Absorbance measurements were performed over wavelength range of 200–800 nm, with particular attention paid to the characteristic absorption peaks of tannic acid and thioctic acid to verify their successful incorporation into the hydrogel matrix.

For  $^{13}\text{C}$  nuclear magnetic resonance (NMR) analysis, freeze-dried hydrogel samples were dissolved in deuterated water ( $\text{D}_2\text{O}$ ) at a concentration of 10 mg/mL. The spectra were recorded using a Bruker 400 MHz NMR spectrometer. The chemical shifts were referenced to the residual solvent peak, and distinct signals corresponding to the carbon atoms in tannic acid and thioctic acid were identified, confirming the

formation of a polymer network.

Raman spectra were acquired using a Thermo Fisher DXR Raman spectrometer with a 532 nm laser. Hydrogel samples were analyzed in their solid form, and spectra were recorded over the range of 400–4000  $\text{cm}^{-1}$ . Particular attention was given to the vibrational modes of the functional groups in tannic acid and thioctic acid. Sulfur-related peaks and polyphenol group signals were identified to confirm hydrogel formation.

Fourier-transform Infrared (FTIR) spectra were acquired using a Nicolet iS10 FTIR spectrometer. Freeze-dried hydrogel samples were mixed with potassium bromide and pressed into pellets for analysis. Spectral data were collected over the range of 400–4000  $\text{cm}^{-1}$ , with particular attention to the characteristic peaks of tannic acid and thioctic acid. Specific peaks corresponding to O–H stretching, C=O stretching, and S–S bonds were analyzed to confirm the chemical interactions underlying the hydrogel formation.

#### 2.3.5. DPPH assay for radical scavenging of the TATA hydrogel

2,2-diphenyl-1-picrylhydrazyl (DPPH, Macklin 1898-66-4) is a well-known stable radical that neutralizes other radicals, making it a standard indicator of radical scavenging activity [52]. In this assay, the reduction in the reaction rate following the introduction of DPPH into the hydrogel reflected its radical scavenging capacity. The evaluation procedure was as follows: 100 mg of freeze-dried TATA Hydrogel was placed in a 50 mL centrifuge tube, to which 30 mL of a 0.15 mmol DPPH/ethanol solution was added. The mixture was incubated in the dark for 30 min. The absorbance at 517 nm was measured using a UV-spectrophotometer, where lower absorbance values corresponded to a higher DPPH scavenging rate. The DPPH scavenging rate was calculated using the following formula:

$$\text{Scavenging activity}\% = \left( \frac{A_c - A_s}{A_c} \right) \times 100\%$$

where,  $A_c$  refers to the absorbance of the control and  $A_s$  represents the absorbance of the sample, with both values measured at 517 nm.

#### 2.3.6. In vivo adhesion evaluation

All animal experiments were approved by the Animal Ethics Committee of Southern Medical University, Guangzhou, and were performed in accordance with the NIH Guide for the Care and Use of Laboratory Animals (NIH Publication No. 85–23, Revised 1985). To evaluate the wound adhesion properties of the TATA Hydrogel, 12 male hemophilic rats (6–8 weeks old,  $200 \pm 20$  g) were used. After the rats were anesthetized, their dorsal hair was shaved, and the skin was sterilized with iodine and alcohol. Four incisions, each 2 cm in length, were made on the dorsal surface of each rat [53,54]. The wounds were subjected to various treatments: no intervention, suture closure (using 4–0 non-absorbable sutures), application of 100  $\mu\text{L}$  TATA Hydrogel (tannic acid and thioctic acid in a 1:1 ratio), and 200  $\mu\text{g}$  of BMSC-derived exosomes combined with 100  $\mu\text{L}$  TATA Hydrogel (1:1 tannic acid to thioctic acid). 7 d post-surgery, the rats were euthanized and  $3 \times 2$  cm skin samples from the wound sites were collected for histological analysis.

#### 2.3.7. Evaluation of antibacterial properties

A 10  $\mu\text{L}$  aliquot of *Escherichia coli* and *Staphylococcus aureus* stock solutions was added to 10 mL of Tryptic Soy Broth (HKM) and incubated at 37 °C for 12 h. After incubation, the bacterial concentration was assessed by measuring the absorbance of the suspension at 600 nm using a UV–Vis spectrophotometer (Thermo Fisher) [55].

The antibacterial activities of the hydrogels were assessed using the inhibition zone method. Cultures of *Escherichia coli* and *Staphylococcus aureus* ( $1 \times 10^5$  CFU/mL) were evenly spread on nutrient agar plates (BKMAMLAB). The cells were divided into three groups: blank control, a tannic acid group, and TATA Hydrogel groups. In the tannic acid group, a circular filter paper disk (1 cm in diameter) soaked in tannic acid

solution was placed at the center of the agar plate after inoculation. For the TATA Hydrogel group, a 1 cm well was created in the center of the agar, into which a TATA Hydrogel (tannic acid and thioctic acid at a 1:1 ratio) was added. After 12 h of incubation at 37 °C, the diameter of the inhibition zone was measured to determine the antibacterial efficacy.

## 2.4. *In vitro* studies

### 2.4.1. Assessment of cell viability and biocompatibility

Live/dead staining, cell counting kit-8 (CCK-8) assay, and cytoskeleton staining were performed to evaluate the *in vitro* biocompatibility of the TATA Hydrogels. For live/dead staining, HUVECs, L929 cells, and RAW264.7 cells were seeded onto TATA Hydrogels at a density of  $5 \times 10^5$  cells per sample and cultured for 24 h. Calcein-AM (Invitrogen, USA) and propidium iodide (PI, Invitrogen, USA) were used as live/dead staining reagents, and PBS was added to each sample, followed by incubation at 37 °C for 30 min. The samples were imaged using a laser scanning confocal microscope (ZEISS LSM 980, Germany). Cell viability was quantified using the CCK-8 assay (Beyotime, China) after 1, 3, and 7 d of culturing. Briefly, 100  $\mu$ L of CCK-8 solution was added to each sample and incubated for 2 h, after which 100  $\mu$ L of supernatant was transferred to a 96-well plate. The optical density (OD) at 450 nm was measured using an ELISA reader (BioTech, Germany), and cell viability was expressed as the ratio of OD values between the experimental and control groups. For cytoskeleton staining, cells were seeded on each sample at a density of  $1 \times 10^5$  cells per well in 12-well plates and cultured for 3 d. Cells were then fixed with 4 % paraformaldehyde and stained with  $\beta$ -Actin Tracker Green (Beyotime, China) and Hoechst (Sigma, USA). Finally, cell morphology was visualized using a laser scanning confocal microscope (ZEISS LSM 980, Germany).

### 2.4.2. Cell migration assay

Fibroblasts play a critical role in soft tissue repair, particularly skin wounds healing [56]. To evaluate the migratory capacity of L929 cells in the presence of exosomes and TATA Hydrogel-Exos, a scratch was introduced onto the surface of the L929 cell cultures upon reaching approximately 90 % confluence, followed by incubation for 12 and 24 h. After incubation, the cultures were rinsed with PBS to remove non-adherent cells, and Calcein AM staining was performed. Cell migration was visualized using an inverted automated microscope (Nikon N31373, Tokyo, Japan).

### 2.4.3. Construction of TATA-Exos hydrogel/RAW264.7 cells/L929 cells co-culture system

To explore whether the immune microenvironment affects the fate of L929 cells, a co-culture system was established using a Transwell chamber (ThermoFisher Scientific, USA) consisting of the TATA-Exos hydrogel, RAW264.7 cells, and L929 cells [56,57]. A polycarbonate membrane with 3.0  $\mu$ m pores was used to separate the compartments, allowing for cytokine exchange. L929 cells ( $1 \times 10^4$ ) were cultured in the upper chamber, while RAW264.7 cells ( $1 \times 10^5$ ) were seeded in the lower chamber. Prior to the co-culture, RAW264.7 cells were pretreated with IL-1 $\beta$  (10 ng/mL) for 24 h, after which the behavior of L929 cells was observed.

### 2.4.4. HUVEC angiogenesis assay

Notably, the promoting of angiogenesis accelerates wound healing [58]. To evaluate the angiogenic potential of HUVECs in the presence of Hydrogel-Exos, HUVECs were seeded onto pre-gelled Matrigel (Corning 354234) at a density of  $1 \times 10^4$  cells per well. The formation of capillary-like structures was monitored and imaged using a laser confocal microscope (ZEISS LSM 980, Germany).

### 2.4.5. Gene expression

Total cellular RNA was extracted using the Simply P Total RNA Extraction Kit (BioFlux, China), and the isolated RNA was reverse

**Table 1**

Primer sequences of each gene.

Target	Forward	Reverse
GAPDH	AACCTTTGGCATTGTGGAAGG	ACACATTGGGGGTAGGAACA
iNOS	CAGCTGGGCTGTACAAACCTT	CATTGGAAGTGAAGCGTTTCG
Arg-1	CTCCAAGCCAAAGTCCTTAGAG	AGGAGCTGTATTAGGGACATC
TNF- $\alpha$	GACCCTCACACTCAGATCATCTTCT	GCTACGACGTGGGCTACAG
IL-10	GACTTTAAGGGTTACCTGGGTTG	TCACATGCGCCTTGATGTCTG

**Table 2**

Characteristics of the primary antibodies.

Antibodies	Species	Type	Dilution (IF/IHC, WB)	Source
Anti-GAPDH	Rabbit	Polyclonal IgG	1:20000	ProteinTech, China
Anti-iNOS	Rabbit	Polyclonal IgG	1:200, 1:1000	ProteinTech, China
Anti-Arg-1	Rabbit	Polyclonal IgG	1:200, 1:5000	ProteinTech, China
Anti-Alix	Rabbit	Polyclonal IgG	1:2000	ProteinTech, China
Anti-CD63	Rabbit	Polyclonal IgG	1:1000	Affinity, China
Anti-TSG101	Mouse	Monoclonal IgG	1:5000	ProteinTech, China
Anti-VEGF	Rabbit	Polyclonal IgG	1:500/1:275, 1:7000	ProteinTech, China
Anti-CD31	Rabbit	Polyclonal IgG	1:10000, 1:4500	ProteinTech, China
Anti-SMA	Rabbit	Polyclonal IgG	1:3750	ProteinTech, China

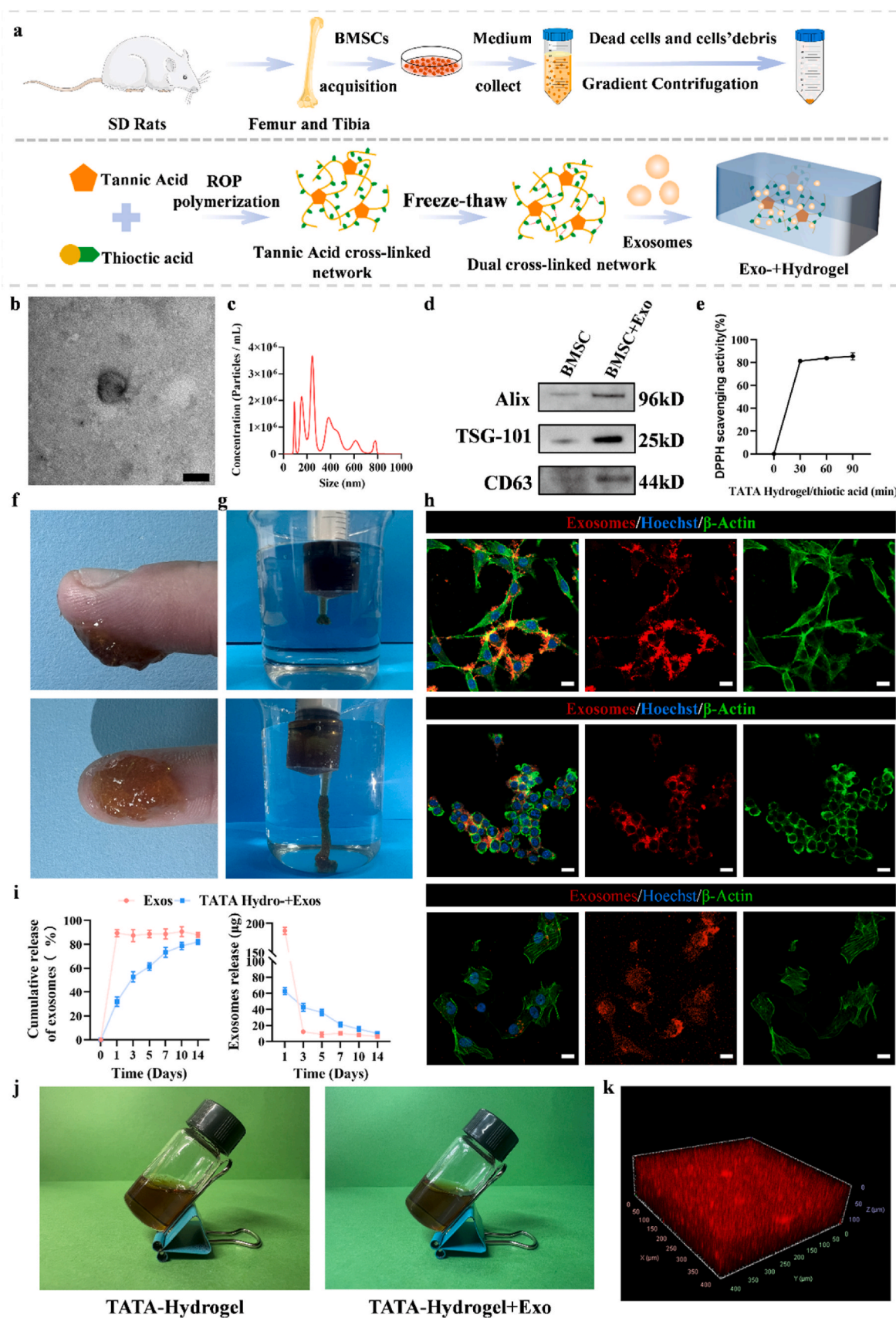
transcribed into cDNA using a reverse transcription kit (TOLOBIO, China). The primers specific to each gene are listed in Table 1. Real-time quantitative PCR (RT-qPCR) was performed using a QuantStudio 5 system (Thermo Fisher Scientific, USA). The experiment was conducted in triplicate, and gene expression analysis was carried out using the  $2^{-\Delta\Delta Ct}$  method for statistical evaluation.

### 2.4.6. Immunofluorescence assay

For the immunofluorescence (IF) assay, the cells were fixed with 4 % paraformaldehyde for 30 min. Following fixation, the cells were permeabilized with 0.5 % Triton X-100 (Biofroxx, Germany) for 30 min and blocked with 3 % bovine serum albumin (BSA, Biofroxx, Germany) for 1 h at room temperature. The cells were subsequently incubated overnight at 4 °C with specific primary antibodies (listed in Table 2, followed by a 1 h incubation at room temperature with secondary antibodies. Hoechst 33342 (Beyotime, China) was used to stain the nuclei for 5 min. Between each step, the samples were washed three times with PBS. Finally, fluorescent images were captured using a laser confocal microscope (ZEISS LSM 980, Germany).

### 2.4.7. Western blotting assay

Cells were lysed in radioimmunoprecipitation assay (RIPA) buffer (CWBI, China) supplemented with protease and phosphatase inhibitors (KeyGEN, China) and maintained on ice for 30 min to extract proteins [59,60]. Total protein concentration was measured using a BCA assay kit (Biovigen, China), and the samples were denatured with loading buffer (Beyotime, China) at 100 °C for 10 min. Equal amounts of protein (20  $\mu$ g) were separated by sodium dodecyl sulfate-polyacrylamide gel electrophoresis (SDS-PAGE, Biovigen, China) and transferred to polyvinylidene fluoride (PVDF) membranes (Thermo Fisher, USA). The membranes were blocked for 15 min using a high efficiency blocking buffer (Genefist, China). Membranes were incubated with primary antibodies (listed in Table 2) were then incubated with the membranes, followed by incubation with secondary antibodies. After immersion in an enhanced chemiluminescence (ECL) solution (Thermo Fisher Scientific, USA), protein bands were visualized using a GelView



(caption on next page)

**Fig. 1.** Characterization and functionalization of the exosomes and hydrogel.

(a) Schematic of the fabrication and structure of Hydrogel-Exos. (b) Transmission electron microscopy (TEM) image illustrating the morphology of the exosomes. Scale bar: 100 nm. (c) Nanoparticle size distribution of the exosomes analyzed by nanoparticle tracking analysis (NTA). (d) Western blotting (WB) of exosome-specific proteins, including TSG101, CD63, and Alix. (e) DPPH assay to assess the antioxidant activity of the hydrogel. (f) Schematic depicting the adhesion of the hydrogel to tissue. (g) Schematic showing the injectability of the hydrogel. (h) Illustration showing the phagocytosis of exosomes by L929 fibroblasts, RAW macrophages, and HUVECs. (i) Depiction of the slow, cumulative release of exosomes from the hydrogel over 14 d. (j) Visual comparison of pure TATA Hydrogel and exosome-loaded hydrogel (20 % w/v) in glass vials at 37 °C. (k) 3D immunofluorescence images demonstrating the uniform distribution of PKH26-labeled exosomes within the adhesive hydrogel, with a penetration depth of approximately 200 μm.

6000 Pro system (BLT, China). The density of the protein bands was quantified using ImageJ software.

## 2.5. *In vivo* experiments

### 2.5.1. Ethical statement

All animal experiments were conducted in accordance with the National Institutes of Health guidelines for the Care and Use of Laboratory Animals. The research protocols were reviewed and approved by the Animal Experimental Ethics Committee of Nanfang Hospital, Southern Medical University.

### 2.5.2. Establishment of the hemophilic rat skin injury model

Adult female FVIII (−/−) rats, weighing 250–300 g, were obtained from the Shanghai Model Organisms Center and genotyped by qPCR using genomic DNA extracted from tail clippings, as described in our previous studies [17,61,62]. Rats were randomly assigned to four groups: an untreated control group (no treatment, n = 10), a pure TATA Hydrogel group (hydrogel, n = 10), suture group (suture, n = 10), and a TATA Hydrogel loaded with exosomes group (TATA Hydrogel-Exos, n = 10). Following anesthesia via an intraperitoneal injection of pentobarbital (40 mg/kg), skin wounds were created. In the hydrogel and Hydrogel-Exos groups, the hydrogel was applied to the wounds using a syringe. In the exosome group, 200 μg of exosomes in PBS were administered directly at the injury site. The suture group underwent interrupted suturing with a 5 mm interval between the stitches. After surgery, all the rats were photographed and allowed to move freely in a warm environment with sufficient food and water.

### 2.5.3. Wound healing assessment

FVIII (−/−) rats were anesthetized using inhaled isoflurane, and photographs of the wounds were captured for documentation purposes. Imaging was performed at designated time points (3, 5, and 7 d post-injury).

### 2.5.4. Hemolysis test and *in vivo* biocompatibility

The blood compatibility of the TATA Hydrogel-Exos was evaluated using a hemolysis assay. Each sample was incubated with whole rat blood at 37 °C for 4 h, using Triton X-100 as a positive control and PBS as a negative control. Following incubation, the samples were centrifuged at 10,000×g for 5 min at 4 °C. The absorbance of the supernatant was measured at 540 nm using a microplate reader (BioTech, Germany), and the hemolysis rate was calculated using the following formula:

$$\text{Hemolysis (\%)} = \frac{\text{OD}_{\text{Sample}} - \text{OD}_{\text{PBS}}}{\text{OD}_{\text{Triton}} - \text{OD}_{\text{PBS}}} \times 100\%$$

where OD represents the optical density.

After 7 d treatment period, alanine aminotransferase (ALT), aspartate aminotransferase (AST), and total protein (TP) levels were measured in whole blood samples to assess the *in vivo* biocompatibility of the treatments. Five major organs (heart, lungs, kidneys, liver, and spleen) were harvested from the rats and subjected to histopathological examination using hematoxylin-eosin (H&E) staining.

## 3. Results

### 3.1. Characterization and functionalization of exosomes and hydrogel

Transmission electron microscopy (TEM) was used to confirm the successful isolation of exosomes from rat BMSCs, revealing their characteristic spherical shape and double-layer membrane structure, which are typical of exosomal vesicles (Fig. 1b). Nanoparticle tracking analysis (NTA) indicated an average particle size of approximately 165.4 ± 79.7 nm, further validating the exosomal identity (Fig. 1c). Western blot analysis demonstrated significant upregulation of exosome-specific surface markers, including TSG101, CD63, and Alix, compared to BMSCs, confirming the successful isolation and enrichment of exosomes (Fig. 1d).

Macroscopic observations demonstrated the strong adhesion of the hydrogel to biological tissues, underscoring its potential for biomedical applications. The hydrogel remained firmly attached to the tissue surface, indicating its robust mechanical properties (Fig. 1f). *In vitro* assessments confirmed its excellent injectability, as the hydrogel could be easily delivered via a syringe while maintaining its structural integrity post-injection, making it suitable for minimally invasive procedures (Fig. 1g). Confocal microscopy revealed a uniform distribution of PKH26-labeled exosomes throughout the hydrogel matrix, confirming successful incorporation and homogeneous dispersion (Fig. 1k). Fluorescent imaging of L929 cells, RAW macrophages, and HUVECs further demonstrated the efficient cellular uptake of PKH26-labeled exosomes, indicating effective exosome delivery from the hydrogel to the cells (Fig. 1h). The cumulative release profiles showed a sustained exosome release, suggesting the potential of the hydrogel for prolonged therapeutic effects through controlled exosome delivery (Fig. 1i). Three-dimensional immunofluorescence imaging revealed the penetration of PKH26-labeled exosomes into the hydrogel to a depth of approximately 200 μm, further confirming the even distribution of exosomes within the matrix (Fig. 1j–k). Additionally, the DPPH assay (Fig. 1e) demonstrated significant antioxidant activity in the TATA Hydrogel, validating its ability to scavenge free radicals and enhancing its potential to mitigate oxidative stress during wound healing.

### 3.2. Rheological and mechanical properties of the hydrogel

UV-visible spectroscopy revealed distinct absorbance peaks for tannic acid and lipoic acid, confirming their successful integration into the hydrogel matrix (Fig. 2a). Rheological analysis demonstrated that the hydrogel maintained its structural integrity under various strain and temperature conditions (25–90 °C), with the storage modulus (G') consistently exceeding the loss modulus (G'') across a range of frequencies, indicating strong mechanical resilience (Fig. 2b and c). Strain scanning tests revealed that the hydrogel could withstand high strain levels (up to 1000 %) without significant deformation. Furthermore, dynamic strain testing confirmed the self-healing capability of the hydrogel, as its original rheological properties were fully restored following substantial strain (500 %), highlighting its potential for long-term durability under physiological conditions (Fig. 2d). These properties suggest that the hydrogel is highly suitable for *in situ* repair of skin injuries.

The self-healing properties of the TATA hydrogel are driven by dynamic disulfide exchange reactions derived from thioctic acid and

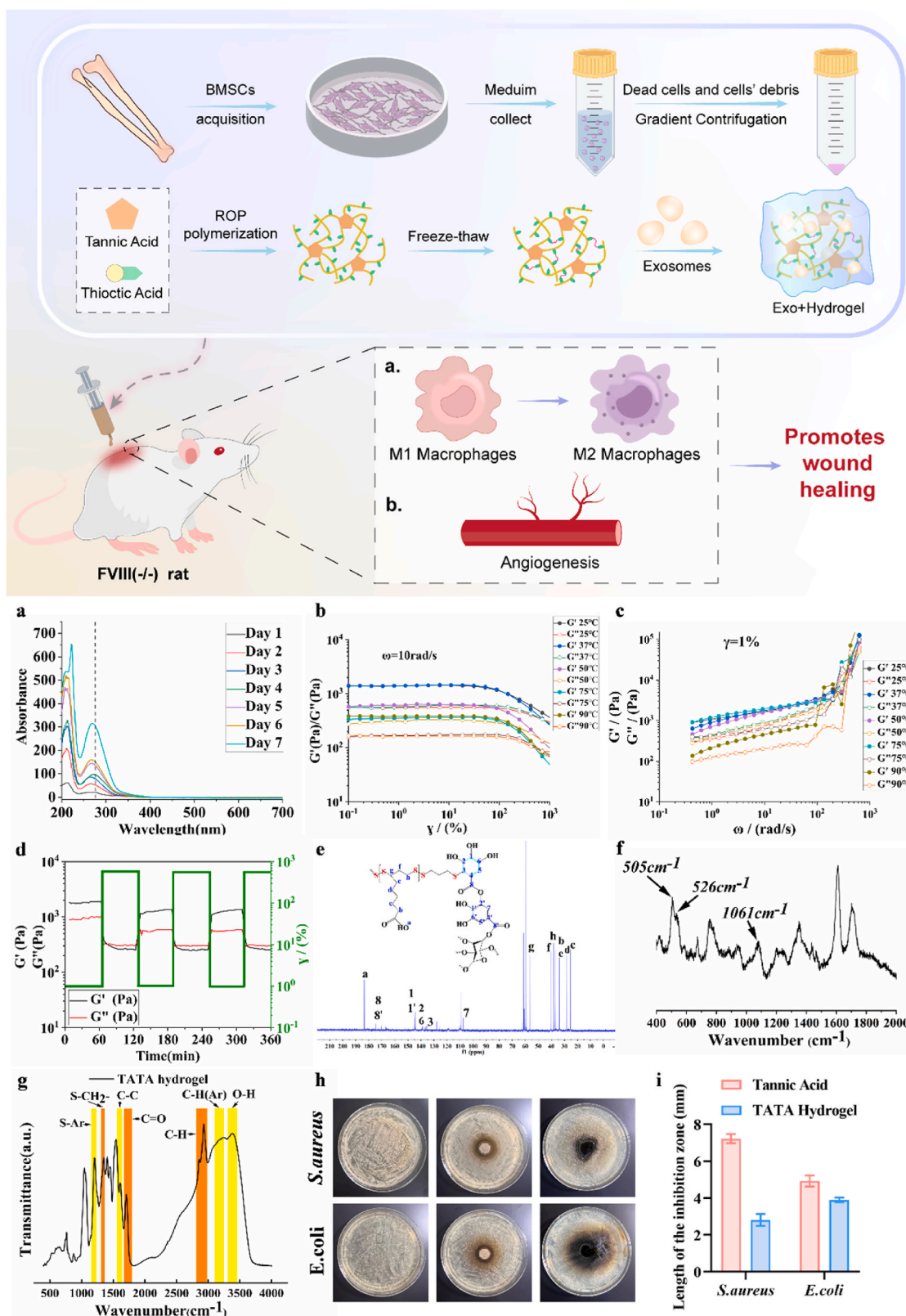
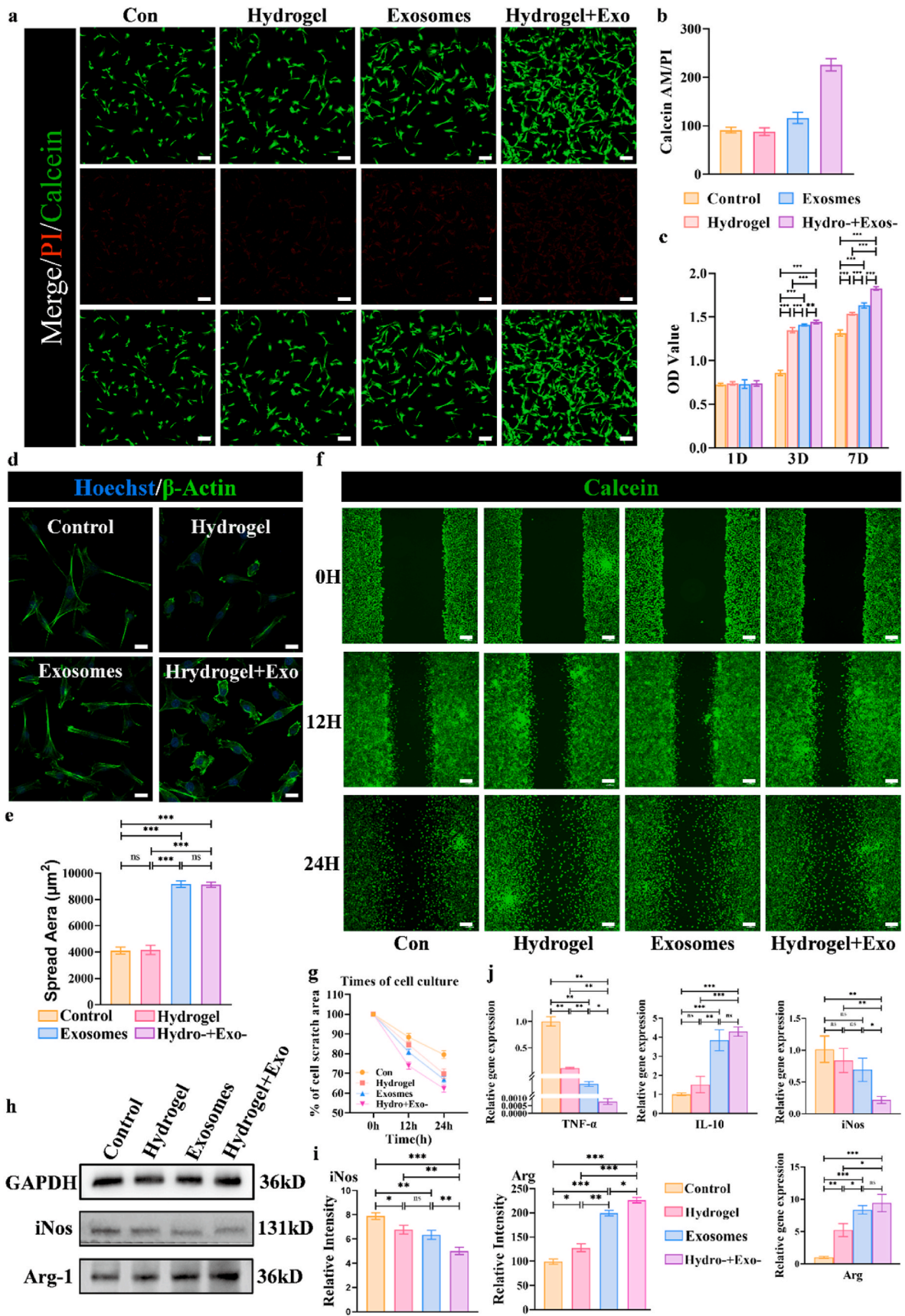


**Fig. 2.** Rheological and mechanical properties of the hydrogel

(a) UV-Vis spectra of the TATA Hydrogel and its oxidation products. (b) Strain sweep measurements of the hydrogel at various temperatures (25, 37, 50, 75, and 90 °C, 10 rad/s). (c) Frequency sweep measurements of the hydrogel across different temperatures (25, 37, 50, 75, and 90 °C, 1 % strain). (d) Repeated dynamic strain step tests ( $\gamma = 1\%$  or 500 %, 10 rad/s) of the hydrogel. (e)  $^{13}\text{C}$  NMR spectra of the hydrogel. (f) Raman spectra of the hydrogel. (g) FTIR spectra of the hydrogel. (h) Antibacterial assays of tannic acid and the hydrogel against *Staphylococcus aureus* and *Escherichia coli*. (i) Quantitative analysis of inhibition zones in the antibacterial assays of tannic acid and the hydrogel.



(caption on next page)



**Fig. 3.** Biological performance of Hydrogel-Exos

(a) Live/dead staining of L929 cells cultured for 1 d across the four groups. The live cells are stained green, and dead cells are stained red. Scale bar: 200  $\mu\text{m}$ . (b) Quantification of live/dead staining ( $n = 3$ ). (c) CCK-8 assay results for each group after 1, 3, and 7 d of cell culturing. (d) Cytoskeleton images showing L929 cell adhesion after 3 d of culturing in each group. Scale bar: 50  $\mu\text{m}$ . (e) Quantification of the cell spreading area ( $n = 5$ ). (f) Wound healing migration assay of L929 cells on each sample at different time points ( $n = 3$ ). Scale bar: 200  $\mu\text{m}$ . (g) Quantitative analysis of scratch area at 0, 12, and 24 h ( $n = 3$ ). (h) Western blot (WB) analysis of iNOS and Arg-1 protein expression. (i) Quantification of iNOS and Arg-1 protein band intensity using ImageJ ( $n = 3$ ). (j) Bar graphs depicting real-time qPCR (RT-qPCR) results for the expression of anti-inflammatory cytokines (Arg-1 and IL-10) and pro-inflammatory cytokines (iNOS and TNF- $\alpha$ ) in each group ( $n = 3$ ). Statistical differences were analyzed using one-way analysis of variance (ANOVA) followed by Bonferroni's multiple comparison test for comparisons between three or more groups. An unpaired *t*-test was used for comparisons between two groups (\* $P < 0.05$ , \*\* $P < 0.01$ , \*\*\* $P < 0.001$ ).

polyphenolic interactions from tannic acid. The reversible disulfide bonds enable the polymer network to reform after mechanical disruption, providing structural recovery. To evaluate the cross-linking density, the hydrogel's swelling ratio was measured as an indirect indicator, with a lower swelling ratio correlating with higher cross-link density. Quantitative swelling analysis revealed that the TATA hydrogel exhibited a swelling ratio of  $230.0 \pm 20.0$  g/g (Fig. S1a), indicating a robust cross-linked network.

Mechanistically, the phenolic groups of tannic acid interact with the thiol groups of thioctic acid, forming covalent and non-covalent bonds, which contribute to the hydrogel's viscoelastic properties. The dynamic nature of these interactions allows the material to autonomously repair microstructural damage. Rheological evaluations further supported this, showing a rapid recovery in storage modulus ( $G'$ ) after applying a high strain of 500 %, indicative of effective network reformation (Fig. 2b–c). These findings directly link the hydrogel's molecular architecture to its self-healing and mechanical durability, providing a deeper understanding of its structural resilience.

The FTIR spectrum, with a peak around  $3649\text{ cm}^{-1}$ , confirmed the presence of hydrogen bonds (Fig. 2g). The absorption peak observed between  $1036$  and  $1059\text{ cm}^{-1}$  in the TATA Hydrogel was attributed to S–Ar bonds, indicating successful crosslinking between tannic acid and thioctic acid through polyphenol–thiyl radical nucleophilic addition. Similarly, the Raman spectrum (Fig. 2f) showed a peak at  $1061\text{ cm}^{-1}$ , corresponding to the S–Ar bond. In the  $^{13}\text{C}$  NMR spectrum (Fig. 2e), the peaks at 144, 110, and 107 ppm were associated with the 1, 3, and 5 aromatic carbons of tannic acid, further confirming the formation of crosslinked structures within the hydrogel [63]. The newly observed peak at 127 ppm is attributed to an Ar–S bond. Additionally, the chemical shifts of the two and six aromatic carbons showed a slight upfield shift (from 137 to 135 ppm), likely because of the increased electron cloud density in the ortho Ar–OH group following the introduction of the thiyl radical. This suggests that during TATA Hydrogel formation, the thiyl radical derived from thioctic acid is likely attached at the 3 or 5 positions of the aromatic carbons. Peaks in the range 25–60 ppm were also observed, corresponding to the aliphatic carbons of poly (thioctic acid).

### 3.3. Biological performance and anti-inflammatory effects of the TATA Hydrogel-Exos

Cell viability assays demonstrated that the hydrogel-Exos group exhibited significantly improved the survival and proliferation of L929 fibroblasts and RAW macrophages, as confirmed by live/dead staining and CCK-8 assays (Fig. 3a–c). Live/dead staining revealed that the majority of cells in the Hydrogel-Exos group were viable (green), with only a small number of dead cells (red), indicating superior biocompatibility (Fig. 3a and b). CCK-8 assays further validated these findings, showing that cells treated with Hydrogel-Exos exhibited markedly higher proliferation rates compared to the control and hydrogel-only groups at 1, 3, and 7 d (Fig. 3c). Cytoskeletal staining revealed enhanced cell adhesion, with cells displaying well-organized cytoskeletal structures and increased spreading on the Hydrogel-Exos surface (Fig. 3d and e). Wound healing assays showed that cells treated with Hydrogel-Exos achieved the highest rates of wound closure at 12 and 24 h, indicating accelerated cell migration (Fig. 3f and g). Western blot and qRT-PCR

analyses confirmed that Hydrogel-Exos promoted M2 macrophage polarization, as demonstrated by increased Arg-1 and IL-10 expression and decreased iNOS and TNF- $\alpha$  levels (Fig. 3h–j), highlighting its anti-inflammatory properties. Immunofluorescence analysis revealed that after lipopolysaccharide stimulation across all groups, RAW264.7 cells treated with TATA-E Hydrogel exhibited a significant increase in M2 macrophage polarization, indicated by elevated Arg-1 expression, and a corresponding decrease in M1 polarization, reflected by reduced iNOS expression, compared to cells treated with either TATA hydrogel or exosomes alone (Figs. S3a–b). In contrast, the lipopolysaccharide-stimulated positive control group predominantly displayed M1 polarization with limited M2 activation. These findings further confirm that the Hydrogel-Exos system effectively promotes a shift toward an anti-inflammatory M2 phenotype, thereby enhancing its therapeutic potential for modulating the inflammatory microenvironment.

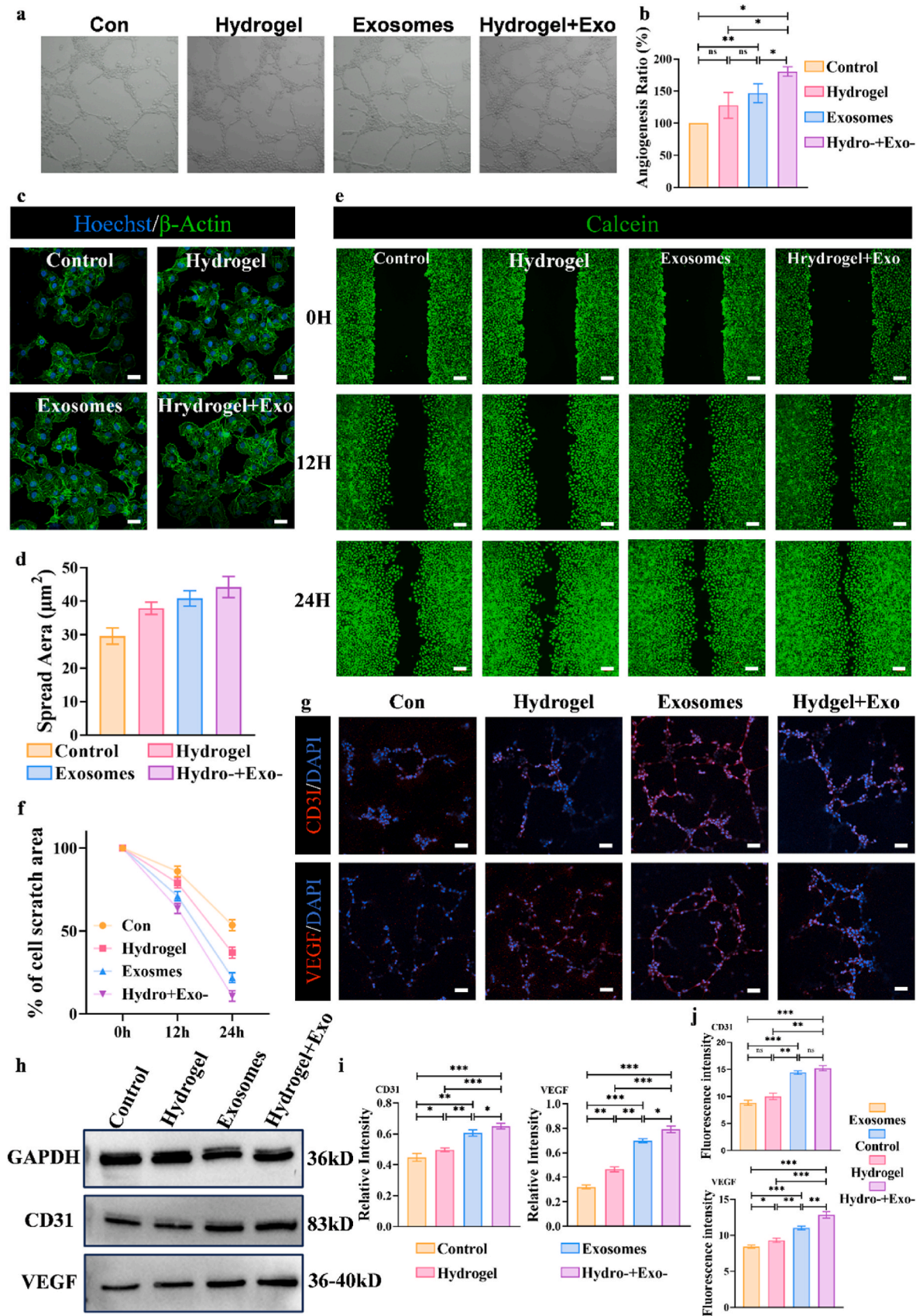
### 3.4. Angiogenic of TATA Hydrogel-Exos

Angiogenesis assays with HUVEC demonstrated significantly enhanced tube formation in the Hydrogel-Exos group compared to the control group, indicating a strong pro-angiogenic effect (Fig. 4a and b). Quantitative analysis of total tube length confirmed the superior angiogenic potential of the hydrogels. Cytoskeletal staining revealed that HUVEC treated with Hydrogel-Exos exhibited increased adhesion and spreading, with a significantly larger spreading area than that in the control group (Fig. 4c and d). Scratch assays showed that Hydrogel-Exos treatment significantly accelerated endothelial cell migration at 12 and 24 h, underscoring its potential to facilitate wound healing (Fig. 4e and f). Immunofluorescence and Western blot analyses further demonstrated that Hydrogel-Exos upregulated the expression of the angiogenic markers CD31 and VEGF, validating the pro-angiogenic capacity of the hydrogel at both the cellular and molecular levels (Fig. 4g–j).

### 3.5. In vivo wound healing and hemostatic performance

In a hemophilic rat model, TATA Hydrogel-Exos exhibited superior hemostatic efficacy across various wound models. In the skin injury model, treatment with TATA Hydrogel-Exos resulted in significantly accelerated wound closure and enhanced tissue regeneration compared to both the control and hydrogel-only groups, as demonstrated by gross images showing complete wound closure (Fig. 5a). In the rat-tail amputation model, the TATA Hydrogel-Exos markedly reduced bleeding time and total blood loss compared to the control and gelatin sponge-treated groups, underscoring its strong hemostatic properties (Fig. 5b and c). Similarly, in the liver hemorrhage model, wounds treated with Hydrogel-Exos displayed faster clot formation and reduced blood loss, and quantitative analysis revealed a significant decrease in both bleeding time and total blood loss compared to the controls (Fig. 5d and e). These findings indicate that TATA Hydrogel-Exos are a highly effective agents for promoting both hemostasis and wound healing under hemophilic conditions.

In addition to its hemostatic efficacy, the TATA Hydrogel-Exos demonstrated excellent biocompatibility and safety. Histological analyses of key organs, including the heart, liver, spleen, lungs, and kidneys, revealed no significant pathological alterations, indicating that the hydrogel did not induce tissue damage or provoke inflammatory



(caption on next page)

**Fig. 4.** Angiogenic analysis of Hydrogel-Exos

(a) Angiogenesis assay of HUVEC cells in each group (n = 3). (b) Quantification of angiogenesis (n = 3). (c) Cytoskeleton images showing HUVEC cell adhesion after 3 d of culturing in each group. Scale bar: 50  $\mu\text{m}$ . (d) Quantification of the cell spreading area (n = 5). (e) Wound healing migration assay of HUVEC cells on each sample at different time points (n = 3). Scale bar: 200  $\mu\text{m}$ . (f) Quantitative analysis of scratch area at 0, 12, and 24 h (n = 3). (g) Immunofluorescence images of CD31 (red) and VEGF (red) in HUVEC cells forming vessels in each group (n = 3). (h) Western blot (WB) analysis of CD31 and VEGF expression. (i) Quantification of CD31 and VEGF protein band intensity using ImageJ (n = 3). (j) Quantitative analysis of immunofluorescence intensity of CD31 and VEGF (n = 3). Statistical differences were assessed using one-way analysis of variance (ANOVA) followed by Bonferroni's multiple comparison test for comparisons among three or more groups. An unpaired *t*-test was used for comparisons between two groups (\**P* < 0.05, \*\**P* < 0.01, \*\*\**P* < 0.001).

responses (Fig. S8a). Additionally, biochemical assessments of liver function markers, such as ALT and AST, showed no significant differences between the Hydrogel-Exos group and controls, further indicating the absence of systemic toxicity (Figs. S8b–d). These results confirm that the Hydrogel-Exos system is biocompatible and safe for biological applications, without adverse effects on vital organs or liver function.

### 3.6. Histological analysis of wound healing

H&E and Masson's trichrome staining of skin tissue sections revealed that wounds treated with Hydrogel-Exos exhibited more organized collagen deposition and enhanced re-epithelialization compared to the control and hydrogel-only groups at 7 d post-treatment (Fig. 6a and b). Quantitative analysis of collagen deposition, based on Masson's staining, demonstrated a significantly higher percentage of collagen coverage in the Hydrogel-Exos group, further supporting its superior regenerative effects (Fig. S3c). The improved tissue architecture in the Hydrogel-Exos group indicated a more advanced stage of healing. Immunohistochemical staining further showed a significant reduction in the pro-inflammatory marker iNOS, along with an increased expression of anti-inflammatory and tissue regeneration markers, including Arg-1, VEGF, and SMA, in Hydrogel-Exos-treated wounds (Fig. 6c and d). These findings suggest that Hydrogel-Exos not only mitigate inflammation but also enhance tissue regeneration and angiogenesis, leading to accelerated wound healing and improved tissue organization.

## 4. Discussion

Hemophilia, a genetic disorder characterized by impaired blood clotting, presents considerable challenges in wound management because of excessive bleeding and delayed tissue repair [1,3]. A key difficulty in treating hemophilic wounds is the inability to form effective clots, which leads to prolonged bleeding. The TATA Hydrogel-Exos developed in this study address these challenges by combining hemostatic properties with enhanced tissue regeneration and modulation of the inflammatory microenvironment. Tannic acid facilitates coagulation, whereas the physical structure of the hydrogel serves as a barrier, reducing both bleeding time and blood loss in *in vitro* and *in vivo* models. Rapid wound stabilization is critical in hemophilia, where even minor injuries can escalate into severe complications.

In addition to its antioxidant properties, the controlled degradation of the hydrogel ensures continuous support throughout the wound healing process without persisting beyond its therapeutic necessity [31]. As healing advances, the hydrogel gradually degrades, eliminating the need for manual extraction, which could otherwise increase the risk of wound reopening and bleeding. The degradation rate can be fine-tuned by adjusting the ratios of tannic acid and thioctic acid, allowing for tailored applications based on the wound types and healing dynamics [31].

The self-healing capacity of the TATA Hydrogel substantially enhances its efficacy in wound care. The dynamic disulfide bonds within its structure allow the hydrogel to autonomously repair itself after mechanical damage, thereby ensuring consistent coverage of the wound site [64]. This feature is particularly beneficial for hemophilic wounds where even minor disturbances to the wound dressing can provoke recurrent bleeding. The ability of a hydrogel to self-repair enables it to maintain its functionality over extended periods, delivering sustained

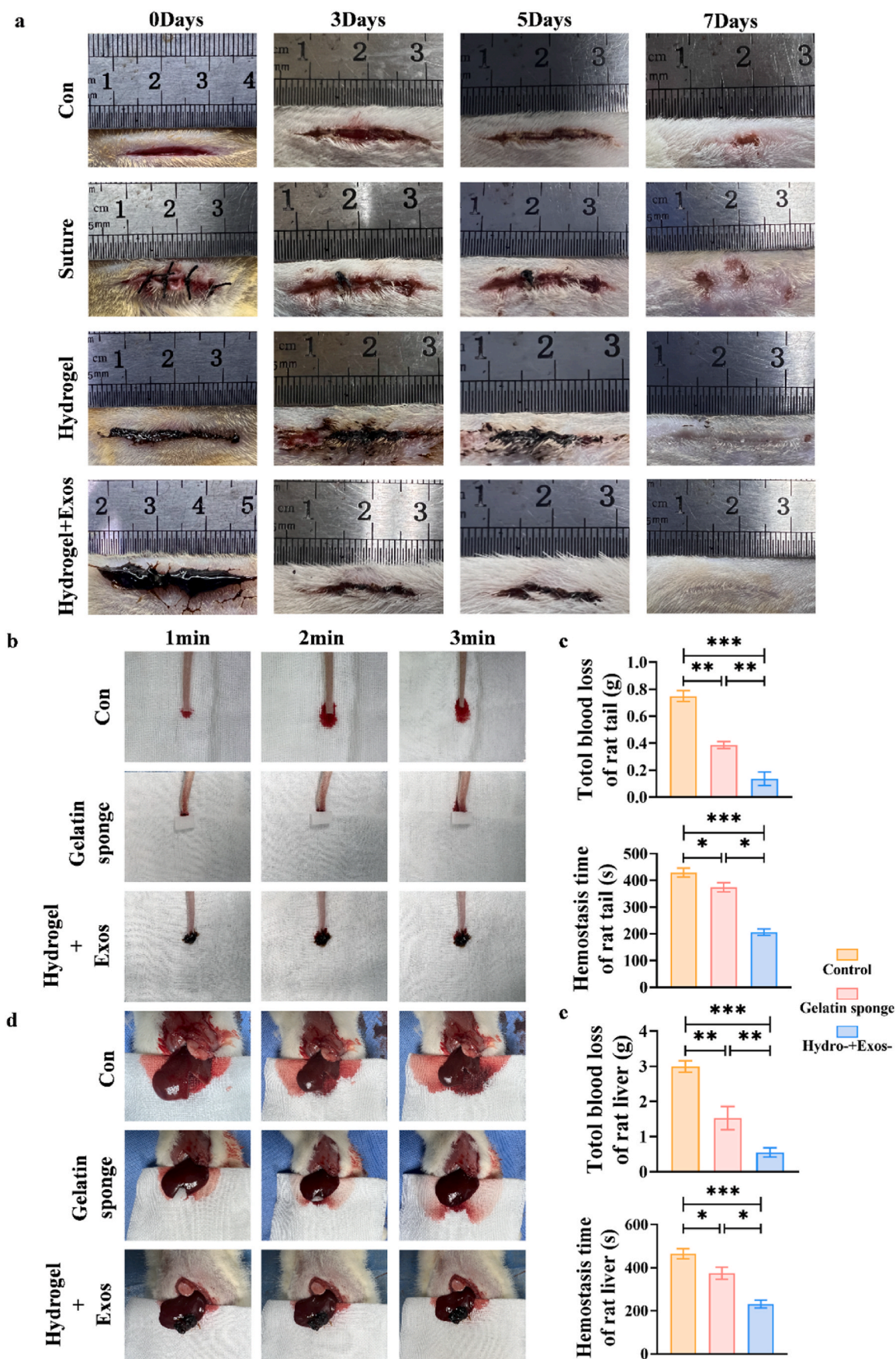
therapeutic effects without the need for frequent reapplication or replacement [65,66].

In addition to their mechanical properties, hydrogels play a crucial role in modulating the inflammatory microenvironment. In hemophilia, excessive or prolonged inflammation can hinder wound healing and increase the risk of chronic wounds or fibrosis [67,68]. The exosome-loaded hydrogel demonstrated its capacity to regulate inflammation by promoting M2 macrophage polarization, as evidenced by elevated levels of anti-inflammatory markers, such as Arg-1 and IL-10, and reduced levels of pro-inflammatory markers, including iNOS and TNF- $\alpha$ . This shift towards an anti-inflammatory, pro-regenerative environment supports tissue repair while minimizing the risk of chronic inflammation. Numerous studies have also confirmed that exosomes derived from BMSCs can modulate immune responses by regulating macrophage phenotypes [69–71].

Tannic acid, thioctic acid-derived disulfide bonds, and exosomes collectively endow the TATA Hydrogel-Exos system with multifunctional capabilities essential for hemophilic wound healing. Tannic acid facilitates coagulation by interacting with tissue proteins and platelet surface receptors, promoting platelet aggregation and adhesion. Its polyphenolic groups oxidize to form quinones, effectively reducing bleeding time and addressing coagulation challenges in hemophilic conditions [22–24]. The hydrogel's self-healing properties arise from dynamic, reversible disulfide bonds that autonomously repair structural disruptions, ensuring consistent wound coverage and maintaining a stable microenvironment conducive to healing [32]. This is particularly critical in hemophilic wounds, where preventing recurrent bleeding is paramount. Furthermore, exosomes incorporated into the hydrogel modulate the inflammatory and regenerative processes by delivering bioactive molecules such as proteins, lipids, and microRNAs to recipient cells [40–42]. This promotes macrophage polarization from a pro-inflammatory M1 phenotype to an anti-inflammatory M2 phenotype, reducing inflammation while supporting tissue repair. Additionally, exosomes enhance angiogenesis by stimulating endothelial cell activity and fibroblast proliferation, thereby accelerating tissue regeneration. Together, these synergistic mechanisms position the TATA Hydrogel-Exos system as a comprehensive solution for hemostasis, inflammation modulation, and tissue repair.

A key advantage of TATA Hydrogel-Exos in wound healing is their ability to promote angiogenesis. Angiogenesis, the formation of new blood vessels, is crucial for delivering oxygen and nutrients to damaged tissues, thereby accelerating the healing process [72,73]. In hemophilic wounds, impaired angiogenesis can further delay healing, because reduced blood flow may lead to ischemia and necrosis [3,73]. The exosomes incorporated into the hydrogel significantly enhanced angiogenic activity, as evidenced by increased tube formation in HUVECs and the upregulation of the angiogenic markers CD31 and VEGF. These results suggest that the hydrogel not only acts as a physical scaffold for wound repair but also provides biological cues that promote neovascularization. This is especially critical in hemophilia, in which impaired angiogenesis can exacerbate delayed healing and tissue necrosis. By stimulating angiogenesis, the TATA Hydrogel effectively addressed this challenge, ensuring adequate vascularization to support the healing process.

*In vivo* experiments using a hemophilic rat model validated the efficacy of the hydrogel. Treatment with Hydrogel-Exos significantly accelerated wound closure, collagen deposition, and re-epithelialization



(caption on next page)

**Fig. 5.** *In vivo* wound healing and hemostatic performance

(a) Gross observation of skin wound healing at 7 d post-treatment. The 'Con' group refers to the untreated control group of hemophilic rats with skin injuries. The 'Suture' group represents the interrupted suturing group, where the sutures were spaced 5 mm apart. The 'Hydrogel' group denotes the treatment group with TATA hydrogel alone. The 'Hydrogel + Exosomes' group corresponds to the treatment group with TATA hydrogel loaded with exosomes. (b) Hemostatic function assessment in the rat tail bleeding model for the control, gelatin sponge, and TATA Hydrogel-Exos groups. (c) Total blood loss and total bleeding time in the rat tail bleeding model ( $n = 3$ ). (d) Hemostatic function assessment in the rat liver hemorrhage model. (e) Total blood loss and total bleeding time in the rat liver hemorrhage model ( $n = 3$ ). Statistical differences were assessed using one-way analysis of variance (ANOVA) followed by Bonferroni's multiple comparison test for comparisons among three or more groups. An unpaired *t*-test was used for comparisons between the two groups (\* $P < 0.05$ , \*\* $P < 0.01$ , \*\*\* $P < 0.001$ ).

compared with the control groups. Histological analysis revealed improved structural organization in the regenerating tissue, indicating that TATA Hydrogel-Exos not only accelerated wound healing but also enhanced the quality of tissue regeneration, resulting in stronger and more resilient skin. This is particularly crucial in hemophilia, where incomplete or fragile tissue repair can lead to recurrent injuries or chronic wounds [3,8]. Moreover, the ability of the hydrogel to promote organized collagen deposition ensures that the newly regenerated tissue possesses the structural integrity necessary to reduce the risk of future tissue breakdown.

In addition to its regenerative properties, the hydrogel exhibited excellent biocompatibility. No significant pathological changes were observed in the major organs of the treated animals, and biochemical analyses revealed no elevation in liver enzymes such as ALT and AST, indicating that the hydrogel did not induce systemic toxicity. This is a critical consideration for clinical applications, especially in chronic conditions, such as hemophilia, where long-term therapeutic use must be both effective and safe. The absence of systemic side effects further highlighted the potential of the TATA hydrogel for future clinical implementation.

Recent advances in biomaterials for wound healing have introduced promising strategies, particularly for conditions like hemophilia, where uncontrolled bleeding and delayed tissue repair are major concerns. In this regard, the development of exosome-loaded hydrogels has gained attention for their ability to modulate inflammation, enhance hemostasis, and promote tissue regeneration [74]. For example, hydrogels enriched with tannic acid and thioctic acid have shown excellent antioxidant and anti-inflammatory properties, essential for managing chronic inflammation that often hampers wound healing. These findings align with recent studies on flexible bioelectronics and tissue engineering, where electrospun fibers have been engineered for controlled release, enhancing tissue regeneration [75]. Moreover, the role of exosomes derived from bone marrow mesenchymal stem cells (BMSCs) in enhancing wound healing is well-documented, as these exosomes facilitate angiogenesis and immune modulation, improving the regenerative capacity of tissues [76]. These parallels findings from recent research on biodegradable nanocatalysts, which have shown that effective modulation of the wound microenvironment can significantly boost wound healing and bacterial defense [77]. Additionally, bioactive materials, such as those discussed in dentin hypersensitivity treatments, also demonstrate the importance of modulating cellular behaviors for effective tissue repair [78]. These studies underscore the growing recognition of biomaterials not only as hemostatic agents but also as multifunctional platforms that address the intricate biological processes critical to wound healing. While these advancements provide strong preclinical evidence, the translation of these materials to clinical settings for hemophilic wound treatment requires further investigation, particularly regarding long-term efficacy and patient-specific adaptations [79, 80].

Despite these promising results, this study had several limitations. First, although the *in vivo* rat model provided valuable insights into hydrogel performance, the long-term effects of TATA Hydrogel-Exos in chronic wound models remain unexamined. Further investigation is needed to assess its efficacy in more complex wound types, such as diabetic ulcers or pressure sores, which present unique healing challenges. Additionally, while TATA Hydrogel-Exos exhibited excellent biocompatibility, as evidenced by the lack of significant changes in liver

enzyme levels (Fig. 6b–d), further toxicological studies are required to confirm their safety for prolonged use in humans. Another area that warrants attention is the optimization the kinetics of exosome release kinetics. Although the hydrogel effectively provided sustained exosome delivery, fine-tuning the release profile to match the different phases of wound healing could further enhance the therapeutic outcomes. This adjustment can be achieved by modifying the tannic acid to thioctic acid ratio, which affects the hydrogel's degradation rate [31]. Moreover, incorporating additional bioactive agents, such as growth factors or antimicrobial peptides, could further enhance the regenerative properties of the hydrogel and broaden its application across diverse wound healing scenarios.

## 5. Summary and conclusion

The exosome-loaded TATA Hydrogel represents a multifunctional therapeutic strategy for addressing the complex challenges of wound healing in patients with hemophilia. By integrating hemostatic properties, antioxidant activity, controlled degradation, self-healing capabilities, inflammation modulation, and angiogenesis promotion, this hydrogel offers a comprehensive solution for both immediate and long-term wound care. Its ability to address critical issues such as excessive bleeding, delayed tissue repair, and impaired blood supply, makes it a promising alternative to existing wound treatments, particularly for patients with bleeding disorders, such as hemophilia.

Future research should focus on optimizing the exosome release kinetics of hydrogels to ensure sustained therapeutic effects throughout the healing process. This can be achieved by fine-tuning the hydrogel composition, such as adjusting the concentration of exosome-loading agents, incorporating biocompatible polymers, or utilizing stimuli-responsive materials that trigger controlled release in response to the wound microenvironment. Investigating its application in other chronic wound types, such as diabetic ulcers and pressure sores, may further enhance its clinical potential. Incorporating other bioactive agents, such as growth factors or antimicrobial peptides, may also improve its therapeutic efficacy and expand the applicability of this hydrogel across diverse wound healing contexts.

To further enhance the clinical applicability of the TATA-Exosomes hydrogel, additional modifications could be explored. Tailoring the hydrogel's mechanical properties to meet the demands of various wound environments, such as enhancing flexibility for irregular wound surfaces or increasing tensile strength for high-stress areas, would improve its versatility. Optimizing the biodegradation rate to synchronize with specific wound healing timelines could further ensure effective support throughout the healing process without requiring premature removal. Additionally, advancing large-scale production techniques to maintain consistency in quality and functionality would facilitate its transition from experimental research to widespread clinical use.

## CRedit authorship contribution statement

**Yuesheng Tu:** Writing – original draft, Validation, Methodology, Conceptualization. **Weixin Zheng:** Formal analysis, Data curation. **Zichu Ding:** Investigation, Formal analysis. **Jie Xiang:** Validation, Methodology. **Qinfeng Yang:** Writing – review & editing. **Yuchen Liu:** Validation, Formal analysis. **Jue Cao:** Validation, Data curation. **Yuling Shen:** Resources, Investigation. **Zinan Tang:** Validation, Formal

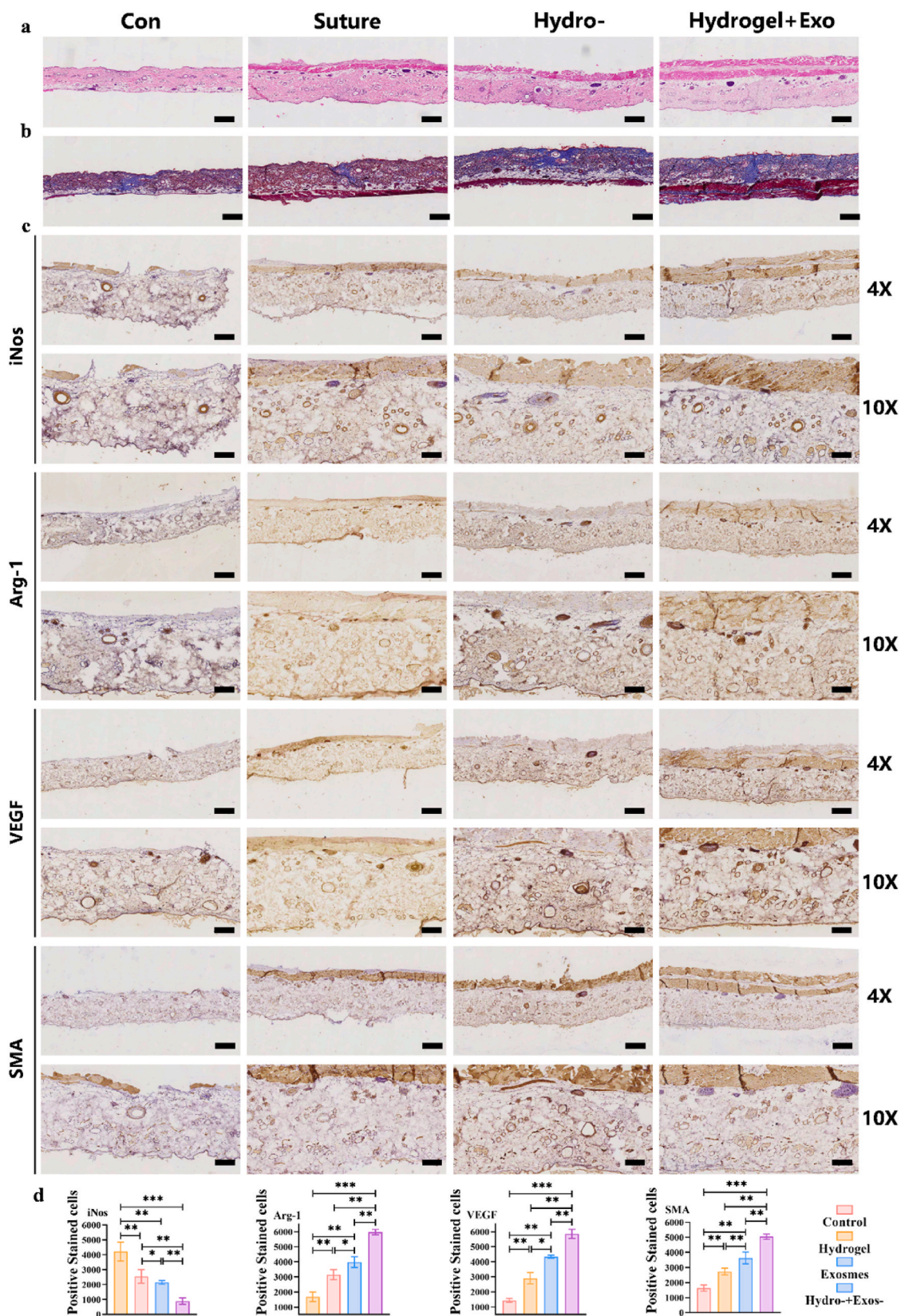


**Fig. 6.** Histological analysis of wound healing

(a) H&E staining of the control, suture, TATA Hydrogel, and TATA Hydrogel-Exos groups at 7 d post-treatment. Scale bar: 312.5  $\mu$ m (low magnification). (b) Masson's trichrome staining of the four groups at 7 d post-treatment. (c) Immunohistochemical staining of iNOS, Arg-1, VEGF, and SMA in the four groups. (d) Quantitative analysis of positive staining for iNOS, Arg-1, VEGF, and SMA in the immunohistochemistry (n = 10). Scale bars: 312.5  $\mu$ m (low magnification), 125  $\mu$ m (medium magnification). Statistical differences were analyzed using one-way analysis of variance (ANOVA) followed by Bonferroni's multiple comparison test for comparisons among three or more groups. An unpaired *t*-test was used for comparisons between the two groups (\**P* < 0.05, \*\**P* < 0.01, \*\*\**P* < 0.001).

analysis. **Shen Lin:** Validation, Investigation. **Lei Fan:** Supervision, Conceptualization. **Yaowen Xu:** Supervision, Project administration. **Bin Chen:** Resources, Project administration, Funding acquisition, Conceptualization.

## Fundings

This research was funded by the National Natural Science Foundation of China (Grant No. 12272164), Innovation Programme among Guangdong, Hong Kong and Macao (2021A0505110011), the Clinical Research Startup Program of Southern Medical University by High-level University Construction Funding of Guangdong Provincial Department of Education (LC2019ZD001), and the Medical Scientific Research Foundation of Guangdong (A2023467).

## Declaration of competing interest

The authors declare that they have no known competing financial interests or personal relationships that could have appeared to influence the work reported in this paper.

## Acknowledgements

We thank Guo Chen for their guidance throughout the research and for their assistance in reviewing the draft of this manuscript.

## Appendix A. Supplementary data

Supplementary data to this article can be found online at <https://doi.org/10.1016/j.mtbio.2025.101496>.

## Data availability

The authors do not have permission to share data.

## References

- [1] K. Nogami, M. Shima, Pathogenesis and treatment of hemophilia, in: E. Ishii (Ed.), *Hematological Disorders in Children: Pathogenesis and Treatment*, Springer Singapore, Singapore, 2017, pp. 189–204.
- [2] C.D. De Brasi, I.R. Slavutsky, I.B. Larriga, [Molecular genetics of hemophilia A], *Medicina* 56 (1996) 509–517.
- [3] M. Hoffman, A. Harger, A. Lenkowski, U. Hedner, H.R. Roberts, D.M. Monroe, Cutaneous wound healing is impaired in hemophilia B, *Blood* 108 (2006) 3053–3060, <https://doi.org/10.1182/blood-2006-05-020495>.
- [4] A.G. McDonald, K. Yang, H.R. Roberts, D.M. Monroe, M. Hoffman, Perivascular tissue factor is down-regulated following cutaneous wounding: implications for bleeding in hemophilia, *Blood* 111 (2008) 2046–2048, <https://doi.org/10.1182/blood-2007-05-092916>.
- [5] J. Chen, M. Kasper, T. Heck, K. Nakagawa, P.M. Humpert, L. Bai, G. Wu, Y. Zhang, T. Luther, M. Andrassy, S. Schiekofer, A. Hamann, M. Morcos, B. Chen, D.M. Stern, P.P. Nawroth, A. Bierhaus, Tissue factor as a link between wounding and tissue repair, *Diabetes* 54 (2005) 2143–2154, <https://doi.org/10.2337/diabetes.54.7.2143>.
- [6] P. Vander Velden, A.R. Giles, A detailed morphological evaluation of the evolution of the haemostatic plug in normal, factor VII and factor VIII deficient dogs, *Br. J. Haematol.* 70 (1988) 345–355, <https://doi.org/10.1111/j.1365-2141.1988.tb02493.x>.
- [7] J.J. Sixma, A. van den Berg, The haemostatic plug in haemophilia A: a morphological study of haemostatic plug formation in bleeding time skin wounds of patients with severe haemophilia A, *Br. J. Haematol.* 58 (1984) 741–753, <https://doi.org/10.1111/j.1365-2141.1984.tb06121.x>.
- [8] D.M. Monroe, M. Hoffman, The clotting system - a major player in wound healing, *Haemophilia* 18 (Suppl 5) (2012) 11–16, <https://doi.org/10.1111/j.1365-2516.2012.02889.x>.
- [9] S. Ellis, E.J. Lin, D. Tartar, Immunology of wound healing, *Current Dermatology Reports* 7 (2018) 350–358, <https://doi.org/10.1007/s13671-018-0234-9>.
- [10] M. Cano Sanchez, S. Lancel, E. Boulanger, R. Neviere, Targeting oxidative stress and mitochondrial dysfunction in the treatment of impaired wound healing: a systematic review, *Antioxidants* 7 (2018), <https://doi.org/10.3390/antiox7080098>.
- [11] Z.-W. Hao, Z.-Y. Zhang, Z.-P. Wang, Y. Wang, J.-Y. Chen, T.-H. Chen, G. Shi, H.-K. Li, J.-W. Wang, M.-C. Dong, L. Hong, J.-F. Li, Bioactive peptides and proteins for tissue repair: microenvironment modulation, rational delivery, and clinical potential, *Mil Med Res* 11 (2024) 75, <https://doi.org/10.1186/s40779-024-00576-x>.
- [12] X. Lin, X. Zhang, Y. Wang, W. Chen, Z. Zhu, S. Wang, Hydrogels and hydrogel-based drug delivery systems for promoting refractory wound healing: applications and prospects, *Int. J. Biol. Macromol.* 285 (2024) 138098, <https://doi.org/10.1016/j.ijbiomac.2024.138098>.
- [13] X. Zhao, Y. Huang, Z. Li, J. Chen, J. Luo, L. Bai, H. Huang, E. Cao, Z. Yin, Y. Han, B. Guo, Injectable self-expanding/self-propelling hydrogel adhesive with procoagulant activity and rapid gelation for lethal massive hemorrhage management, *Adv Mater* 36 (2024) e2308701, <https://doi.org/10.1002/adma.202308701>.
- [14] Z. Xu, W. Tian, C. Wen, X. Ji, H. Diao, Y. Hou, J. Fan, Z. Liu, T. Ji, F. Sun, D. Wu, J. Zhang, Cellulose-based cryogel microspheres with nanoporous and controllable wrinkled morphologies for rapid hemostasis, *Nano Lett.* 22 (2022) 6350–6358, <https://doi.org/10.1021/acs.nanolett.2c02144>.
- [15] H.-C. Horng, W.-H. Chang, C.-C. Yeh, B.-S. Huang, C.-P. Chang, Y.-J. Chen, K.-H. Tsui, P.-H. Wang, Estrogen effects on wound healing, *Int. J. Mol. Sci.* 18 (2017), <https://doi.org/10.3390/ijms18112325>.
- [16] E. Rendra, V. Riabov, D.M. Mossel, T. Sevastyanova, M.C. Harmsen, J. Kzhyshkowska, Reactive oxygen species (ROS) in macrophage activation and function in diabetes, *Immunobiology* 224 (2019) 242–253, <https://doi.org/10.1016/j.imbio.2018.11.010>.
- [17] Q. Yang, G. Liu, G. Chen, G. Chen, K. Chen, L. Fan, Y. Tu, J. Chen, Z. Shi, C. Chen, S. Liu, G. Deng, X. Deng, C. Sun, X. Li, S. Yang, S. Zheng, B. Chen, Novel injectable adhesive hydrogel loaded with exosomes for holistic repair of hemophilic articular cartilage defect, *Bioact. Mater.* 42 (2024), <https://doi.org/10.1016/j.bioactmat.2024.08.018>.
- [18] K. Kalantari, E. Mostafavi, B. Saleh, P. Soltantabar, T.J. Webster, Chitosan/PVA hydrogels incorporated with green synthesized cerium oxide nanoparticles for wound healing applications, *Eur. Polym. J.* 134 (2020) 109853, <https://doi.org/10.1016/j.eurpolymj.2020.109853>.
- [19] V. Dediu, J. Ghitman, G. Gradisteanu Pircalabioru, K.H. Chan, F.S. Iliescu, C. Iliescu, Trends in photothermal nanostructures for antimicrobial applications, *Int. J. Mol. Sci.* 24 (2023), <https://doi.org/10.3390/ijms24119375>.
- [20] P. Wang, F. Cai, Y. Li, X. Yang, R. Feng, H. Lu, X. Bai, J. Han, Emerging trends in the application of hydrogel-based biomaterials for enhanced wound healing: a literature review, *Int. J. Biol. Macromol.* 261 (2024) 129300, <https://doi.org/10.1016/j.ijbiomac.2024.129300>.
- [21] W. Zhang, R. Wang, Z. Sun, X. Zhu, Q. Zhao, T. Zhang, A. Cholewinski, F.K. Yang, B. Zhao, R. Pinnaratip, P.K. Forooshani, B.P. Lee, Catechol-functionalized hydrogels: biomimetic design, adhesion mechanism, and biomedical applications, *Chem. Soc. Rev.* 49 (2020) 433–464, <https://doi.org/10.1039/c9cs00285e>.
- [22] J. Guo, W. Sun, J.P. Kim, X. Lu, Q. Li, M. Lin, O. Mrowczynski, E.B. Rizk, J. Cheng, G. Qian, J. Yang, Development of tannin-inspired antimicrobial bioadhesives, *Acta Biomater.* 72 (2018) 35–44, <https://doi.org/10.1016/j.actbio.2018.03.008>.
- [23] J. Park, T.Y. Kim, Y. Kim, S. An, K.S. Kim, M. Kang, S.A. Kim, J. Kim, J. Lee, S.-W. Cho, J. Seo, A mechanically resilient and tissue-conformable hydrogel with hemostatic and antibacterial capabilities for wound care, *Adv. Sci.* 10 (2023) e2303651, <https://doi.org/10.1002/adv.202303651>.
- [24] C. Chai, P. Zhang, L. Ma, Q. Fan, Z. Liu, X. Cheng, Y. Zhao, W. Li, J. Hao, Regenerative antibacterial hydrogels from medicinal molecule for diabetic wound repair, *Bioact. Mater.* 25 (2023) 541–554, <https://doi.org/10.1016/j.bioactmat.2022.07.020>.
- [25] A.K.B. Bedran-Russo, K.J. Yoo, K.C. Ema, D.H. Pashley, Mechanical properties of tannic-acid-treated dentin matrix, *J. Dent. Res.* 88 (2009) 807–811, <https://doi.org/10.1177/0022034509342556>.
- [26] X. Zhang, M.D. Do, P. Casey, A. Sulistio, G.G. Qiao, L. Lundin, P. Lillford, S. Kosaraju, Chemical modification of gelatin by a natural phenolic cross-linker, tannic acid, *J. Agric. Food Chem.* 58 (2010) 6809–6815, <https://doi.org/10.1021/jf1004226>.
- [27] G. Strauss, S.M. Gibson, Plant phenolics as cross-linkers of gelatin gels and gelatin-based coacervates for use as food ingredients, *Food Hydrocolloids* 18 (2004) 81–89, [https://doi.org/10.1016/S0268-005X\(03\)00045-6](https://doi.org/10.1016/S0268-005X(03)00045-6).
- [28] S. Peng, S. Niu, Q. Gao, R. Song, Z. Wang, Z. Luo, X. Zhang, X. Qin, Hydroxypropyl chitosan/e-poly-L-lysine based injectable and self-healing hydrogels with antimicrobial and hemostatic activity for wound repair, *Carbohydr. Polym.* 337 (2024) 122135, <https://doi.org/10.1016/j.carbpol.2024.122135>.
- [29] J. Zhou, M. Penna, Z. Lin, Y. Han, R.P.M. Lafleur, Y. Qu, J.J. Richardson, I. Yarovsky, J.V. Jakerst, F. Caruso, Robust and versatile coatings engineered via simultaneous covalent and noncovalent interactions, *Angew. Chem. Int. Ed. Engl.* 60 (2021) 20225–20230, <https://doi.org/10.1002/anie.202106316>.
- [30] S. Betharia, A.N. Rondon-Ortiz, D.A. Brown, Disubstituted dithiolethione ACDT exerts neuroprotective effects against 6-hydroxydopamine-induced oxidative stress in SH-SY5Y cells, *Neurochem. Res.* 44 (2019) 1878–1892, <https://doi.org/10.1007/s11064-019-02823-3>.
- [31] C. Chen, X. Yang, S. Li, C. Zhang, Y. Ma, Y. Ma, P. Gao, S. Gao, X.-J. Huang, Tannic acid-thioctic acid hydrogel: a novel injectable supramolecular adhesive gel for wound healing, *Green Chem.* 23 (2021), <https://doi.org/10.1039/D0GC02909B>.
- [32] K. Endo, T. Yamanaka, Copolymerization of lipoic acid with 1,2-dithiane and characterization of the copolymer as an interlocked cyclic polymer, *Macromolecules* 39 (2006) 4038–4043, <https://doi.org/10.1021/ma060063n>.
- [33] X. Zhang, R.M. Waymouth, 1,2-Dithiolane-Derived dynamic, covalent materials: cooperative self-assembly and reversible cross-linking, *J. Am. Chem. Soc.* 139 (2017) 3822–3833, <https://doi.org/10.1021/jacs.7b00039>.
- [34] Y. Li, J. Wang, Y. Ma, W. Du, K. Feng, S. Wang, miR-101-loaded exosomes secreted by bone marrow mesenchymal stem cells requires the FBXW7/HIF1 $\alpha$ /FOXp3 axis,

- facilitating osteogenic differentiation, *J. Cell. Physiol.* 236 (2021) 4258–4272, <https://doi.org/10.1002/jcp.30027>.
- [35] S.M. Richardson, G. Kalamegam, P.N. Pushparaj, C. Matta, A. Memic, A. Khademhosseini, R. Mobasheri, F.L. Poletti, J.A. Hoyland, A. Mobasheri, Mesenchymal stem cells in regenerative medicine: focus on articular cartilage and intervertebral disc regeneration, *Methods* 99 (2016) 69–80, <https://doi.org/10.1016/j.ymeth.2015.09.015>.
- [36] X. Shen, J. Qin, Z. Wei, F. Liu, Bone marrow mesenchymal stem cell exosome-derived lncRNA TUC339 influences the progression of osteoarthritis by regulating synovial macrophage polarization and chondrocyte apoptosis, *Biomed. Pharmacother.* 167 (2023) 115488, <https://doi.org/10.1016/j.biopha.2023.115488>.
- [37] G. Liang, Y. Feng, W. Tang, L. Yao, C. Huang, Y. Chen, Proinflammatory bone marrow mesenchymal stem cell-derived exosomal miR-150-3p suppresses proinflammatory polarization of alveolar macrophages in sepsis by targeting inhibin subunit beta A, *J. Interferon Cytokine Res.* 43 (2023) 518–530, <https://doi.org/10.1089/jir.2023.0068>.
- [38] S. Chu, T. Yu, W. Wang, H. Wu, F. Zhu, C. Wei, F. Gao, C. Liu, H. Fan, Exosomes derived from EphB2-overexpressing bone marrow mesenchymal stem cells regulate immune balance and repair barrier function, *Biotechnol. Lett.* 45 (2023) 601–617, <https://doi.org/10.1007/s10529-023-03358-y>.
- [39] Y. Chen, Y. Wu, L. Guo, S. Yuan, J. Sun, K. Zhao, J. Wang, R. An, Exosomal lnc NEAT1 from endothelial cells promote bone regeneration by regulating macrophage polarization via DDX3X/NLRP3 axis, *J. Nanobiotechnology* 21 (2023) 98, <https://doi.org/10.1186/s12951-023-01855-w>.
- [40] W. Liao, Y. Du, C. Zhang, F. Pan, Y. Yao, T. Zhang, Q. Peng, Exosomes: the next generation of endogenous nanomaterials for advanced drug delivery and therapy, *Acta Biomater.* 86 (2019), <https://doi.org/10.1016/j.actbio.2018.12.045>.
- [41] J.-W. Choi, J.-H. Um, J.-H. Cho, H.-J. Lee, Tiny RNAs and their voyage via extracellular vesicles: secretion of bacterial small RNA and eukaryotic microRNA, *Exp Biol Med (Maywood)* 242 (2017) 1475–1481, <https://doi.org/10.1177/1535370217723166>.
- [42] R. Kalluri, V.S. LeBleu, The biology, function, and biomedical applications of exosomes, *Science* 367 (2020), <https://doi.org/10.1126/science.aau6977>.
- [43] M. Colombo, G. Raposo, C. Théry, Biogenesis, secretion, and intercellular interactions of exosomes and other extracellular vesicles, *Annu. Rev. Cell Dev. Biol.* 30 (2014) 255–289, <https://doi.org/10.1146/annurev-cellbio-101512-122326>.
- [44] Z. Wang, Y. Wu, Z. Zhao, C. Liu, L. Zhang, Study on transorgan regulation of intervertebral disc and extra-skeletal organs through exosomes derived from bone marrow mesenchymal stem cells, *Front. Cell Dev. Biol.* 9 (2021) 741183, <https://doi.org/10.3389/fcell.2021.741183>.
- [45] R. Zhang, J. Ma, J. Han, W. Zhang, J. Ma, Mesenchymal stem cell related therapies for cartilage lesions and osteoarthritis, *Am J Transl Res* 11 (2019) 6275–6289.
- [46] Z.-F. Han, J.-H. Cao, Z.-Y. Liu, Z. Yang, R.-X. Qi, H.-L. Xu, Exosomal lncRNA KLF3-AS1 derived from bone marrow mesenchymal stem cells stimulates angiogenesis to promote diabetic cutaneous wound healing, *Diabetes Res. Clin. Pract.* 183 (2022) 109126, <https://doi.org/10.1016/j.diabres.2021.109126>.
- [47] F.-X. Zhang, P. Liu, W. Ding, Q.-B. Meng, D.-H. Su, Q.-C. Zhang, R.-X. Lian, B.-Q. Yu, M.-D. Zhao, J. Dong, Y.-L. Li, L.-B. Jiang, Injectable Mussel-Inspired highly adhesive hydrogel with exosomes for endogenous cell recruitment and cartilage defect regeneration, *Biomaterials* 278 (2021) 121169, <https://doi.org/10.1016/j.biomaterials.2021.121169>.
- [48] L. Li, Y. Zhang, J. Mu, J. Chen, C. Zhang, H. Cao, J. Gao, Transplantation of human mesenchymal stem-cell-derived exosomes immobilized in an adhesive hydrogel for effective treatment of spinal cord injury, *Nano Lett.* 20 (2020) 4298–4305, <https://doi.org/10.1021/acs.nanolett.0c00929>.
- [49] Q. Li, H. Yu, M. Sun, P. Yang, X. Hu, Y. Ao, J. Cheng, The tissue origin effect of extracellular vesicles on cartilage and bone regeneration, *Acta Biomater.* 125 (2021) 253–266, <https://doi.org/10.1016/j.actbio.2021.02.039>.
- [50] L. Bonjoch, V. Casas, M. Carrascal, D. Closa, Involvement of exosomes in lung inflammation associated with experimental acute pancreatitis, *J. Pathol.* 240 (2016) 235–245, <https://doi.org/10.1002/path.4771>.
- [51] M. Regato-Herbella, I. Morhenn, D. Mantione, G. Pascuzzi, A. Gallastegui, A. B. Caribé Dos Santos Valle, S.E. Moya, M. Criado-Gonzalez, D. Mecerreyes, ROS-responsive 4D printable acrylic thioether-based hydrogels for smart drug release, *Chem. Mater.* 36 (2024) 1262–1272, <https://doi.org/10.1021/acs.chemmater.3c02264>.
- [52] Í. Gulcin, S.H. Alwasel, DPPH radical scavenging assay, *Processes* (2023).
- [53] P. Wang, Y. Pu, Y. Ren, S. Liu, R. Yang, X. Tan, W. Zhang, T. Shi, S. Li, B. Chi, Bio-inspired hydrogel-based bandage with robust adhesive and antibacterial abilities for skin closure, *Sci. China Mater.* 65 (2022) 246–254, <https://doi.org/10.1007/s40843-021-1724-8>.
- [54] Y. Tian, P. Guan, C. Wen, M. Lu, T. Li, L. Fan, Q. Yang, Y. Guan, X. Kang, Y. Jiang, C. Ning, R. Fu, G. Tan, L. Zhou, Strong biopolymer-based nanocomposite hydrogel adhesives with removability and reusability for damaged tissue closure and healing, *ACS Appl. Mater. Interfaces* 14 (2022) 54488–54499, <https://doi.org/10.1021/acsami.2c14103>.
- [55] R. Du, D. Yang, X. Yin, Rapid detection of three common bacteria based on fluorescence spectroscopy, *Sensors* 22 (2022), <https://doi.org/10.3390/s22031168>.
- [56] S. Zhang, D. Li, H. Wang, B. Liu, F. Du, Q. Wang, CAFs-derived exosomal miR-889-3p might repress M1 macrophage polarization to boost ESCC development by regulating STAT1, *Cell Biochem. Biophys.* (2024), <https://doi.org/10.1007/s12013-024-01496-2>.
- [57] Y. Mu, X. Zhang, L. Zhang, R. Luo, Y. Zhang, M. Wang, MSC exosomes containing valproic acid promote wound healing by modulating inflammation and angiogenesis, *Molecules* 29 (2024), <https://doi.org/10.3390/molecules29174281>.
- [58] Y. Sun, S. Zhang, Y. Shen, H. Lu, X. Zhao, X. Wang, Y. Wang, T. Wang, B. Liu, L. Yao, J. Wen, Therapeutic application of mesenchymal stem cell-derived exosomes in skin wound healing, *Front. Bioeng. Biotechnol.* 12 (2024) 1428793, <https://doi.org/10.3389/fbioe.2024.1428793>.
- [59] S. Yang, J. Xie, Z. Pan, H. Guan, Y. Tu, Y. Ye, S. Huang, S. Fu, K. Li, Z. Huang, X. Li, Z. Shi, L. Li, Y. Zhang, Advanced glycation end products promote meniscal calcification by activating the mTOR-ATF4 positive feedback loop, *Exp. Mol. Med.* 56 (2024) 630–645, <https://doi.org/10.1038/s12276-024-01190-6>.
- [60] P. Guan, C. Liu, D. Xie, S. Mao, Y. Ji, Y. Lin, Z. Chen, Q. Wang, L. Fan, Y. Sun, Exosome-loaded extracellular matrix-mimic hydrogel with anti-inflammatory property Facilitates/promotes growth plate injury repair, *Bioact. Mater.* 10 (2022) 145–158, <https://doi.org/10.1016/j.bioactmat.2021.09.010>.
- [61] K.R. Sørensen, K. Roepstorff, B. Wiinberg, A.K. Hansen, M. Tranholm, L.N. Nielsen, M. Kjølgaard-Hansen, The F8(-/-) rat as a model of hemophilic arthropathy, *J Thromb Haemost* 14 (2016) 1216–1225, <https://doi.org/10.1111/jth.13328>.
- [62] J. Magisetty, U.R. Pendurthi, C.T. Esmol, L.V.M. Rao, EPCR deficiency or function-blocking antibody protects against joint bleeding-induced pathology in hemophilia mice, *Blood* 135 (2020) 2211–2223, <https://doi.org/10.1182/blood.2019003824>.
- [63] T.J. Kim, J.L. Silva, M.K. Kim, Y.S. Jung, Enhanced antioxidant capacity and antimicrobial activity of tannic acid by thermal processing, *Food Chem.* 118 (2010) 740–746, <https://doi.org/10.1016/j.foodchem.2009.05.060>.
- [64] Y. Wang, Q. Chen, M. Chen, Y. Guan, Y. Zhang, PHEMA hydrogel films crosslinked with dynamic disulfide bonds: synthesis, swelling-induced mechanical instability and self-healing, *Polym. Chem.* 10 (2019) 4844–4851, <https://doi.org/10.1039/C9PY00670B>.
- [65] M.M.H. Rumon, A.A. Akib, F. Sultana, M. Moniruzzaman, M.S. Niloy, M.S. Shakil, C.K. Roy, Self-healing hydrogels: development, biomedical applications, and challenges, *Polymers* 14 (2022), <https://doi.org/10.3390/polym14214539>.
- [66] H. Omidian, R.L. Wilson, E.J. Gill, Advancements and challenges in self-healing hydrogels for wound Care, *Gels* 10 (2024), <https://doi.org/10.3390/gels10040241>.
- [67] M. Li, Q. Hou, L. Zhong, Y. Zhao, X. Fu, Macrophage related chronic inflammation in non-healing wounds, *Front. Immunol.* 12 (2021) 681710, <https://doi.org/10.3389/fimmu.2021.681710>.
- [68] P. Schillrreff, U. Alexiev, Chronic inflammation in non-healing skin wounds and promising natural bioactive compounds treatment, *Int. J. Mol. Sci.* 23 (2022), <https://doi.org/10.3390/ijms23094928>.
- [69] S. Zhang, C. Lu, S. Zheng, G. Hong, Hydrogel loaded with bone marrow stromal cell-derived exosomes promotes bone regeneration by inhibiting inflammatory responses and angiogenesis, *World J Stem Cells* 16 (2024) 499–511, <https://doi.org/10.4252/wjsc.v16.i5.499>.
- [70] J. Du, Y. Dong, J. Song, H. Shui, C. Xiao, Y. Hu, S. Zhou, S. Wang, BMSC-derived exosome-mediated miR-25-3p delivery protects against myocardial ischemia/reperfusion injury by constraining M1-like macrophage polarization, *Mol. Med. Rep.* 30 (2024), <https://doi.org/10.3892/mmr.2024.13266>.
- [71] X. Zhou, C. Ye, L. Jiang, X. Zhu, F. Zhou, M. Xia, Y. Chen, The bone mesenchymal stem cell-derived exosomal miR-146a-5p promotes diabetic wound healing in mice via macrophage M1/M2 polarization, *Mol. Cell. Endocrinol.* 579 (2024) 112089, <https://doi.org/10.1016/j.mce.2023.112089>.
- [72] Z. Shi, C. Yao, Y. Shui, S. Li, H. Yan, Research progress on the mechanism of angiogenesis in wound repair and regeneration, *Front. Physiol.* 14 (2023) 1284981, <https://doi.org/10.3389/fphys.2023.1284981>.
- [73] H. Thittamaranahalli Muguregowda, K. Pramod, U. Echalarasa Govindarama Padmanabha, K. Sudesh, K. Udaya, R. Pragna, Role of angiogenesis and angiogenic factors in acute and chronic wound healing, *Plastic and Aesthetic Research* 2 (2015) 243–249, <https://doi.org/10.4103/2347-9264.165438>.
- [74] R. Li, K. Liu, X. Huang, D. Li, J. Ding, B. Liu, X. Chen, Bioactive materials promote wound healing through modulation of cell behaviors, *Adv. Sci.* 9 (2022) e2105152, <https://doi.org/10.1002/adv.202105152>.
- [75] X. Wan, Y. Zhao, Z. Li, L. Li, Emerging polymeric electrospun fibers: from structural diversity to application in flexible bioelectronics and tissue engineering, *Exploration (Beijing)* 2 (2022) 20210029, <https://doi.org/10.1002/EXP.20210029>.
- [76] Q. Luo, Z. Li, B. Liu, J. Ding, Hydrogel formulations for orthotopic treatment of myocardial infarction, *Expert Opin Drug Deliv* 21 (2024) 1463–1478, <https://doi.org/10.1080/17425247.2024.2409906>.
- [77] X. Wang, C. Ding, Z. Zhang, C. Li, D. Cao, L. Zhao, G. Deng, Y. Luo, C. Yuan, J. Lu, X. Liu, Degradable nanocatalyst enables antitumor/antibacterial therapy and promotion of wound healing for diabetes via self-enhanced cascading reaction, *Chin. Chem. Lett.* 34 (2023) 107951, <https://doi.org/10.1016/j.ccl.2022.107951>.
- [78] Q. Wang, J. Luan, Z. Zhao, W. Kong, C. Zhang, J. Ding, Dentin-desensitizing biomaterials, *Chin. Chem. Lett.* 34 (2023) 108060, <https://doi.org/10.1016/j.ccl.2022.108060>.
- [79] H. Gao, L. Zhang, X. Lian, Y. Wang, S. Jiang, G. Wang, X. Dai, H. Zou, D. Ding, A dentin hypersensitivity treatment using highly stable photothermal conversion nanoparticles, *Mater. Chem. Front.* 5 (2021) 3388–3395, <https://doi.org/10.1039/DOQM01006E>.
- [80] Y. Peng, Y. Zhuang, Y. Liu, H. Le, D. Li, M. Zhang, K. Liu, Y. Zhang, J. Zuo, J. Ding, Bioinspired gradient scaffolds for osteochondral tissue engineering, *Exploration (Beijing)* 3 (2023) 20210043, <https://doi.org/10.1002/EXP.20210043>.